Postprint of: Khalifa M. E., El Azab, I. H., Gobouri, A. A., Mersal, G. A.M., Alharthi S., Saracoglu M., Kandemirli F., Ryl J., Amin M. A., Adsorption behavior and corrosion inhibitive characteristics of newly synthesized cyano-benzylidene xanthenes on copper/sodium hydroxide interface: Electrochemical, X-ray photoelectron spectroscopy and theoretical studies, Journal of Colloid and Interface Science Vol. 580 (2020); pp 108-125 DOI: 10.1016/j.jcis.2020.06.110

Adsorption behavior and corrosion inhibitive characteristics of newly synthesized cyano-benzylidene xanthenes on copper/sodium hydroxide interface: Electrochemical, X-ray photoelectron spectroscopy and theoretical studies

Mohamed E. Khalifa[a*], Islam H. El Azab[a,b], Adil A. Gobouri[a], Gaber A.M. Mersal[a,c], Sarah Alharthi[a], Murat Saracoglu[d], Fatma Kandemirli[e], Jacek Ryl[f], Mohammed A. Amin[a,g*]

[a]*Department of Chemistry, Faculty of Science, Taif University, Al-Haweiah, P.O. Box 888, Taif 21974, Saudi Arabia*

[b]*On leave from department of Chemistry, Faculty of Science, Aswan University, Aswan, P.O. box 81528, Aswan, Egypt*

[c]*Chemistry Department, Faculty of Science, South Valley University, Qena, Egypt*

[d]*Erciyes University, Faculty of Education, 38039, Kayseri, Turkey*

[e]*Kastamonu University, Faculty of Engineering and Architecture, Department of Biomedical Engineering, 37150, Kastamonu, Turkey*

[f]*Department of Electrochemistry, Corrosion and Materials Engineering, Faculty of Chemistry, Gdansk University of Technology, Narutowicza 11/12, 80-233 Gdansk, Poland*

[g]*Department of Chemistry, Faculty of Science, Ain Shams University, 11566 Abbassia, Cairo, Egypt*

Corresponding Authors:

Prof.Mohamed E. Khalifa (mohamedezzat200@hotmail.com)

Prof. Mohammed A. Amin (maaismail@yahoo.com)

Abstract: Elegant process for synthesis of 3-(7*H*-dibenzo[*c*,*h*]xanthen-7-yl)benzaldehyde**(3)**, as new starting material to create a set of novel xanthene analogues, 2-(3-(7H-dibenzo[c,h]xanthen-7-yl)benzylidene)malononitrile**(4)**, 3-(3-(7H-dibenzo[c,h]xanthen-7-yl)phenyl)-2-cyanoacrylic acid**(5)**, and Ethyl-3-(3-(7H-dibenzo[c,h]xanthen-7-yl)phenyl)-2-cyanoacrylate**(6)**, was achieved starting with available materials under mild conditions. Various concentrations (ca. 0.1–1.0 mM) of the synthesized cyano-benzylidene xanthene derivatives, namely compounds **3, 4, 5, and 6**, were tested as inhibitors to control copper corrosion in alkaline solutions employing polarization and electrochemical impedance spectroscopy (EIS) measurements. Results revealed that the four studied xanthenes derivatives served as efficient (mixed-type) inhibitors. The inhibition efficiency increased with increase in inhibitor concentration. The inhibition performance of studied compounds varied according to their chemical structures. The best inhibitor, compound **5**, achieved a maximum inhibition efficiency of 98.7% (calculated from corrosion current densities for uninhibited and inhibited solutions) and ~95% (estimated from charge-transfer resistance values) at a concentration of 1.0 mM. The morphology of the corroded and inhibited copper surfaces was studied by scanning electron microscopy (SEM). The adsorption of the inhibitor molecules was confirmed by high-resolution X-ray photoelectron spectroscopy (XPS) profiles. XPS data were used to compare the inhibition efficiencies exhibited by studied compounds. The oxidation rate of the Cu surface was found to be frivolous, referring to high inhibition efficiency, only in the presence of inhibitor **(5)**, and Cu^0 share is 87% of all copper components. The shares of Cu^0 were significantly reduced to 43%, 26% and 20% for inhibitors **(3)**, **(4)** and **(6)**, respectively. These findings go parallel with the results obtained from electrochemical measurements. The quantum-chemical calculations of the investigated molecules were performed to support electrochemical findings, and their correlations with the inhibition efficiency of the synthesized compounds were discussed.

Keywords: Xanthene dyes; Adsorption; Copper corrosion inhibition; Electrochemical measurements; XPS; Quantum chemical calculations.

1. Introduction

Copper (Cu), one of the most abundant metals in the earth's crust, is useful and highly applied in a pure or alloying form. The most important, and well-known, Cu alloys are brass, Cu-Ni and bronze. High electrical and thermal conductivity, mechanical workability, and malleability are the most favourable characteristics of copper [1] that made it widely used in various industrial applications [2, 3]. Cu is also atmospheric and aqueous corrosion-resistant due to the formation of protective layers of passive Cu-oxides and/or nonconductive corrosion products on its surface [4, 5].

However, Cu corrodes readily in aqueous media containing oxygen and some anions such as chloride, sulfate, and hydroxide [6, 7]. Cu corrosion and subsequent formation of corrosion products have undesired impacts on the performance of the applied Cu-based systems, reducing their efficiency [8]. For these reasons, numerous corrosion-research groups worldwide devoted themselves toward elaborating new organic compounds as efficient inhibitors for Cu corrosion in a variety of harsh aqueous environments. For instance, azoles [3,9-15], thiols [16, 17], amino acids [18-20], surfactants [21-25], and phytic acid and its salts [26-28], and many others [29, 30], served as typical organic inhibitors for Cu corrosion. Most of these efficient inhibitors are organic compounds containing N, S, O, and P as heteroatoms that are capable of donating electrons to the vacant d-orbitals of the Cu atoms, forming coordinate covalent bonds [29, 30]. In the same time, such compounds can accept free electrons from the Cu atom using their anti-bonding molecular orbitals forming feedback bonds [29, 30].

Xanthene and its derivatives (xanthenes) are one of the most important classes of heterocyclic compounds exhibiting various pharmacological characteristics such as antibacterial, antiviral, anti-inflammatory and fungicide [31-34]. Xanthenes also acted as effective corrosion inhibitors for the acid corrosion of mild steel [35-37]. To the best of our knowledge, there are no articles on xanthenes as inhibitors for the aqueous corrosion of copper. From here comes the objective of the present work, which

explores the use of our newly synthesized xanthene derivatives as promising inhibitors for the corrosion of Cu in NaOH solutions.

The choice of xanthenes for this work was based on the consideration that it contains several benzene rings that are fused together. The π electrons of these rings are delocalized over all their carbon atoms thus, constituting together a pool of electrons. In addition, the new xanthene derivatives synthesized here contain polar functional groups, namely –CN, –COOEt, and –COOH including nitrogen and oxygen heteroatoms. All these features of the chemical structure of our newly synthesized xanthene derivatives can induce greater adsorption of the inhibitor molecule onto the surface of copper [38].

The objective here is to study the inhibition performance of such newly synthesized xanthene derivatives towards the alkaline corrosion of Cu. Measurements were conducted in naturally aerated 1.0 M NaOH solution using various electrochemical techniques. Morphology and chemistry of the corroded and inhibited Cu surfaces were investigated by SEM and XPS examinations. Theoretical calculations, employing several quantum chemical methods and molecular modelling techniques, were also performed to support the experimental findings.

1. Experimental

1.1. Materials and methods

Both chemicals and reagents, supplied by Sigma Aldrich Co., Darmstadt, Germany, were analytical grade or chemically pure.IR spectra were conducted in the Micro Analytical Center (MAC) at Taif University (Taif, Saudi Arabia).Other spectral analyses, namely 1H NMR, 13C NMR, MS and elemental analysis were performed at Mansoura University (Mansoura, Egypt).Methodology and instrumentations used were previously reported [39], and discussed in depth in *Section* S1 (Supplementary Information).

1.2. Synthesis

1.2.1. Synthesis of 3-(7H-dibenzo[c,h]xanthen-7-yl)benzaldehyde(3).

A mixture of isophthaldehyde**(1,** 0.01 mole, 1.34 gm) and two moles of 2-naphthol**(2**, 0.02 mole, 2.88 gm) in presence of oxalic acid solution as a catalyst (0.01 mole, 0.99 gm) was stirred and warmedat 80 °C on water bath for 40 min. The reaction mixture was poured on ice-cold H_2O. The isolated solid product was filtered off, washed with MeOH and then recrystallized from EtOH to afford **3**, in 63% yield as faint yellow powder; mp. 85–90 °C. IR: ν (cm^{-1}), 3264 (=CH Ar), 1688 (C=O aldehydic) and 1209 (C–O xanthene ring); ^{1}H NMR (DMSO–d_6):5.88 (s, 1H, Pyran–H4), 7.09–7.56 (m, 12H, Ar–H); 10.14 (s, 1H, CHO). ^{13}C NMR:49.9 (CH–Pyran.), 118.1, 120.3, 122.4, 125.5, 125.6, 126.1, 126.3, 127.3, 132.6, 150.1 (20 C=C Naphth.), 127.3, 129.3, 129.6, 134.1, 140.1, 142.63 (C=C–Phenyl), 191.1 (C=O);MS (*m/z*, %): 387.13 (M+1, 30.4). Anal. Calcd. for $C_{28}H_{18}O_2$ (386.44) C, 87.02; H, 4.69, O, 8.28%. Found: C, 87.18; H, 4.79, O, 8.10%.

1.2.2. General procedure for synthesis of 7-phenyl-7H-dibenzo[c,h]xanthene derivatives(4-6).

A mixture of xanthene derivative (**3**, 0.01 mole, 3.86 gm), in dry EtOH (30 mL) containing 0.2 mL of piperidine as catalyst, and molar ratio of active methylenecompoundsnamely; malononitrile, cyanoacetic acid and ethylcyanoacetate, was stirred at ambient temperature for 2 hr. The reaction mixture was poured onto acidified ice-cold H_2O. The isolated precipitates were filtered off, washed with H_2O, dried well, and recrystallized from EtOH to afford *dibenzo[c,h]xanthene* derivatives **(4**–**6),** respectively.

2.2.2.1. 2-(3-(7H-dibenzo[c,h]xanthen-7-yl)benzylidene)malononitrile(4). Yield: 71%; mp. 180–182 °C.IR: ν (cm^{-1}), 3329 (=CH Ar), 2188 (C≡N_{str}.) and 1223 (C-O xanthene ring);^{1}H NMR (DMSO–d_6):5.86 (s, 1H, Pyran–H4), 7.08–7.64(m, 15H, Ar-H; s, 1H, olefinic proton);^{13}C NMR:49.9 (CH–Pyran.), 81. 4, 161.3 (C=C olefinic), 113.6 (2 CN), 118.1, 120.3, 122.4, 125.5, 125.6, 126.1, 126.3, 127.3, 132.6, 150.1 (20 C=C Naphth.), 125.8, 126.1, 127.3, 129.1, 135.6, 141.6 (C=C–Phenyl); MS (*m/z*, %): 434.14 (M^+,100.0). Anal. Calc. for $C_{31}H_{18}N_2O$ (434.49) C, 85.69; H, 4.18; N, 6.45; O, 3.68 %. Found: C, 85.37; H, 4.01; N, 6.02; O, 3.31 %.

2.2.2.2. 3-(3-(7H-dibenzo[c,h]xanthen-7-yl)phenyl)-2-cyanoacrylic acid(5). Yield: 73%; mp. 110–112 °C.IR: ν (cm^{-1}), 3392 (br, OH), 2200 (C≡N_{str}.), 1264 (C–O xanthene ring) and 1611 (CO acid); ^{1}H NMR:5.86 (s, 1H, Pyran–H4), 7.08-7.64 (s, 15H, Ar–H; s, 1H, olefinic proton), 12.11 (s, 1H, COOH);^{13}C NMR:49.9 (CH–Pyran.), 86.6, 157.3 (C=C olefinic), 117.6 (CN), 118.1, 120.3, 122.4, 125.5, 125.6, 126.1, 126.3, 127.3, 132.6, 150.1 (20 C=C Naphth.), 125.8, 126.1, 127.3, 129.1, 135.6, 141.6 (C=C–Phenyl), 159.7 (C=O);MS (*m/z*, %): 453.14 (M^+, 100). Anal. Calc. for $C_{31}H_{19}NO_3$ (453.49) C, 82.10; H, 4.22; N, 3.09; O, 10.58 %. Found: C, 82.15; H, 4.56; N, 2.77; O, 10.19 %.

2.2.2.3. Ethyl-3-(3-(7H-dibenzo[c,h]xanthen-7-yl)phenyl)-2-cyanoacrylate(6). Yield: 73%; mp. 248–250 °C.IR: ν (cm^{-1}), 3214(=CH Ar), 2205, (C≡N_{str}.), 1709 (C=O_{str}. ester), 1476 (CH_2) and 1365 (CH_3); ^{1}H NMR: 1.05 (t, 3H, Me), 4.43 (q, 2H, CH_2),5.86 (s, 1H, Pyran–H4), 7.08–7.64 (s, 15H, Ar-H; s, 1H, olefinic proton);^{13}C NMR:14.1 (Me), 49.9 (CH-Pyran.), 60.8 (CH_2), 120.6, 154.5 (C=C olefinic), 117.6 (CN), 118.1, 120.3, 122.4, 125.5, 125.6, 126.1, 126.3, 127.3, 132.6, 150.1 (20 C=C Naphth.), 125.8, 126.1, 127.3, 129.1, 135.6, 141.6 (C=C-Phenyl), 159.7 (C=O);MS (*m/z*, %): 481.17 (M^+, 30.12). Anal. Calc. for $C_{33}H_{23}NO_3$ (481.54) C, 82.31; H, 4.81; N, 2.91; O, 9.97 %. Found: C, 82.15; H, 4.56; N, 3.27; O, 9.68 %.

Electrochemical measurements

The working electrode (WE) employed in this work is made from a pure copper rode (99.99%). For electrochemical measurements, the copper rode was mounted into a Teflon jacket providing an apparent cross-sectional area of 0.50 cm^2. Prior to each electrochemical run, the WE was subjected to various steps of mechanical polishing and rinsing as previously reported [25] followed by etching in 7.0 M HNO_3 solution, adopting the method of B.V. Appa Rao *et al*. [40].

Electrochemical measurements were conducted using an electrochemical setup composed of a standard double jacketed Pyrex electrochemical cell, with a long spiral platinum wire counter electrode and a Ag/AgCl reference electrode, connected to a potentiostat/galvanostat AUTOLAB (PGSTAT30). This potentiostat/galvanostat instrument is coupled with an Autolab frequency response analyzer (FRA) with FRA2 module connected to PC. Electrochemical characterizations were carried out in a 200 mL volume cell containing naturally aerated NaOH solutions (1.0 M) without and with various concentrations (0.1–1.0 mM) of the four tested inhibitors **(3-6)** at 25 ^oC ± 0.2. The chemical structure of the four synthesized inhibitors is depicted in **Fig. 1**.

Tafel polarization and EIS techniques were employed to evaluate the inhibition performance of the studied compounds towards the alkaline corrosion of Cu. EIS measurements were conducted at the respective corrosion potential, E_{corr}, covering a wide range of frequency (100 *kHz*–1.0 *mHz*) using AC signals of amplitude 5 mV peak-to-peak. EIS was followed by Tafel polarization measurements, where the potential of the WE (E_{WE}) was swept within the potential of the Tafel region ($E_{WE} = E_{corr}$ ± 250 mV) at 5.0 mV s^{-1} scan rate.

The inhibited solutions were prepared by first dissolving in 1.0 mL acetone at ambient temperature, and then the corrosive medium (1.0 M NaOH) was added thoroughly with continuous stirring.

2.3. SEM and XPS examinations of the corroded and inhibited Cu surfaces

The topography of Cu samples resulted from the exposure in alkaline environment in the absence and presence of studied corrosion inhibitors was evaluated by Scanning Electron Microscopy (SEM), utilizing S-3400N (Hitachi, Japan) microscope. The micrographs were carried out in secondary electron mode, with 20 kV accelerating voltage. The X-Ray Photoelectron Spectroscopy (XPS) examinations were carried out on Escalab 250Xi (ThermoFisher Scientific, UK), equipped with monochromator. 20 eV pass energy and 0.1 eV energy step size were applied to conduct high-resolution XPS analyses. The spectra were constructed in the energy range of *Cu2p*$_{3/2}$, *O1s*, *C1s* and *N1s*.Charge compensation was controlled using a flood gun through the low-energy electron and low-energy Ar^+ ion emission.

2.4. Computational studies

The molecules of the four synthesized cyano-benzylidene xanthene derivatives were theoretically investigated, and their quantum chemical parameters were rendered using Gaussian 09 (Revision A.02),using the DFT/B3LYPexchange-correlationfunction withstandard6-311G(d,p) basis set [41]. More details are reported in the Supplementary Information file, *Section* S2.

3. Results and Discussion

3.1. Chemistry

Multi component's condensation in the presence of a Brönsted or Lewis acid is the key synthetic method employed for xanthene preparation [42]. Recently, the multi-component processes (MCRs) have gained significant economic and environmental interest, as they have been shown to be a very elegant and quick way of accessing complex structures from basic building blocks in a single synthetic operation, and display high atomic efficiency and high selectivity[43]. Thus, isophthaldehyde**(1)** was allowed to reactwith two moles of 2-naphthol**(2)**, in presence of catalytic amount of oxalic acid to yield the 3-(7*H*-dibenzo[*c*,*h*]xanthen-7-yl)benzaldehyde**(3)**,as shown in Scheme 1.

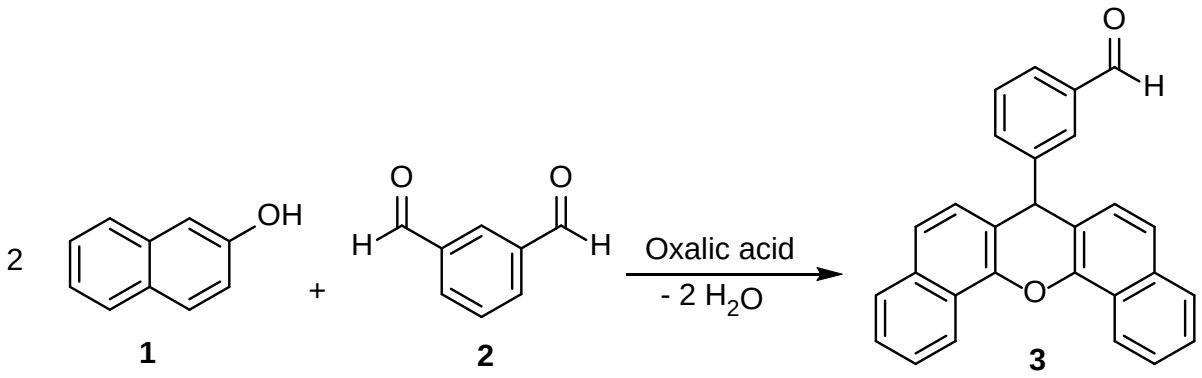

Scheme 1. Synthesis of 3-(7*H*-dibenzo[*c*,*h*]xanthen-7-yl)benzaldehyde**(3)**

The structure of the xanthene aldehyde derivative **(3)** was elucidated by means of its spectral and elemental analyses (c.f. experimental section).

The xanthenylbenzaldehyde**(3)** was integrated into a series of investigations to explore its formyl tag's reactivity to create the target compounds. Thus, it was easily condensed with different active methylene compounds (i.e. malononitrile, cyanoacetic acid and ethylcyanoacetate) under basic conditions

to afford the motive nitrile derivatives **(4–6)**, respectively as described in **Scheme 2**. Isolated product structures **(4–6)** were elucidated by spectral data along with their proper elementary analysis (c.f. **Figs.** 2-4 and experimental section). For instance, the IR spectra of the isolated products displayed the absorption bands in the regions 2188–2205 cm^{-1} due to $C{\equiv}N_{str.}$, group. The signal of the formyl proton originally observed in compound **(3)** at 9.87 ppm in ^1H NMR spectra was disappeared in compound **5**, besides the appearance of two new singlet peaks at 7.93 and 12.11 ppm attributed to the olefinic and carboxylic protons, respectively. The mass spectrum of **(5)** displayed an intense peak at *m/z*453.14 (M^+, 100%) corresponding to the expected molecular formula $C_{31}H_{19}NO_3$.

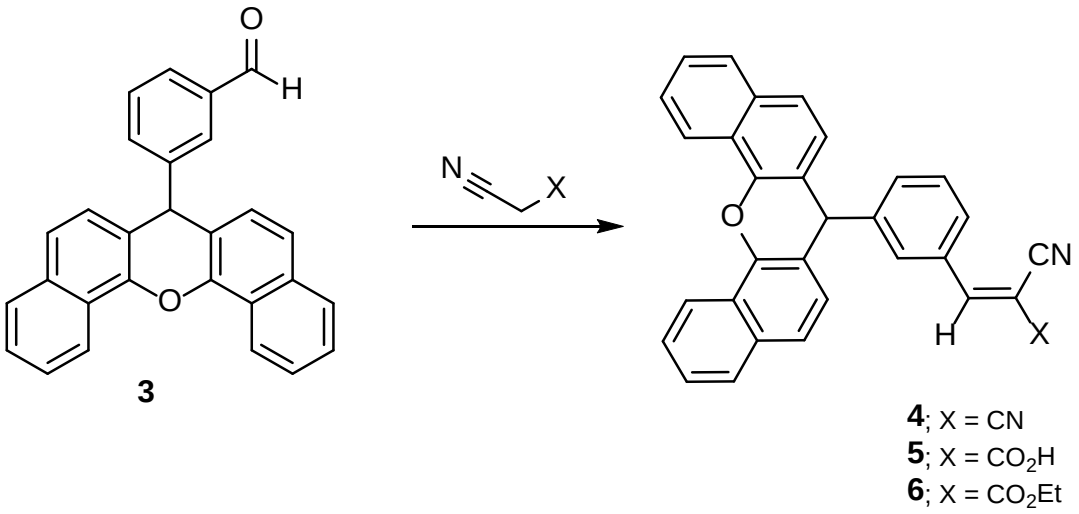

Scheme 2. Synthesis of 2-(4-(12*H*-dibenzo[*c*]xanthen-7-yl)benzylidene) derivatives **(4-6)**

3.2. Electrochemical studies

3.2.1. Polarization measurements

Fig. 5 shows the cathodic and anodic polarization curves recorded for Cu in 1.0 M NaOH solutions without and with different concentrations (ca. 0.1 – 1.0 mM) of studied inhibitors. Tafel extrapolation method was applied, as described elsewhere [44], to extract the various electrochemical kinetic parameters associated

with such polarization measurements (Table 1). A representative example demonstrating how the Tafel extrapolation method is applied is shown in **Fig. S1** (**Supporting Information**). The parameters include in Table 1 are corrosion current densities (j_{corr}), corrosion potential (E_{corr}), and anodic Tafel slope (β_a). Cathodic Tafel slope (β_c) cannot be accurately determined due to diffusion limitations (reduction of dissolved oxygen under diffusion control) within the cathodic branch of the polarization curves [20,45,46].

The inhibition efficiency values (ε%) calculated from Eq. (1) are also included in **Table 1**.

$$\varepsilon\% = \left\{\frac{jo-ji}{jo}\right\} \times 100 \qquad (1)$$

where j_o and j_i denote the corrosion current density values in the absence and presence of the inhibitor, respectively. The presence of any of the tested inhibitors shifted both of the cathodic and anodic branches towards lower currents with no significant changes in E_{corr}. These results demonstrated that the four studied compounds act as mixed-type inhibitors for the alkaline corrosion of Cu, mitigating corrosion *via* adsorption on the cathodic and anodic sites. An eminent decrease in j_{corr} can be observed in the presence of such inhibitors. The extent of this decrease in j_{corr} depends upon the concentration and type of the additive. At any concentration of the studied inhibitors, the lowest j_{corr} value was recorded for inhibitor **(5)**, which exhibited a maximum inhibition efficiency of 98.7% at a concentration of 1.0 mM.

*3.2.2. **EIS measurements (Cu/OH/Xanthenes)***

Fig. 6 shows the Nyquist impedance plots measured for Cu in naturally aerated NaOH solution (1.0 M) devoid of and containing various concentrations (ca. 0.1–1.0 mM) of the studied inhibitors. Measurements were conducted at the respective E_{corr} at 298 K. In the blank solution, the Cu electrode exhibited an impedance response characterized by a depressed semicircle at the high frequencies (HF), followed by a straight line at 45° at low frequency values (LF). The appearance of the Warburg impedance Z_W (diffusion tail) in the LF region referred to the corrosion process controlled by diffusion [20,45,46]. This process

involved the diffusion of the electro-active species, such as the corrosive OH^- species or dissolved oxygen, from the solution bulk to the metal surface at the Cu/electrolyte interface or the transportation of soluble corrosion products in the reverse direction [20,45,46]. In presence of the inhibitor, the Z_W gradually disappears at the analysed LF region and the diameter of the capacitive loop markedly increases versus that is measured in the blank solution. These findings confirm the high inhibition performance of the studied inhibitors. The extent of these events depends on the type and concentration of the tested inhibitor and well pronounced at higher inhibitor's concentrations. These results suggest that the diffusion of the corrosive species is significantly delayed as a result of the inhibitor's protective film formation. This leaves behind charge transfer as the main process controlling the corrosion of copper in these solutions.

When fitting the impedance data with electric equivalent circuit, a model with singular time-constant was utilized. The HF capacitive semicircle was assigned to a charge transfer process involving parallel charge transfer resistance R_{ct} through the electrode/electrolyte interface and charge accumulation by the corrosion inhibitor film and the double layer. The depressed nature of the capacitive loop, due to the frequency dispersion resulting from adsorbed film heterogeneity and other Cu surface non-heterogeneities,was represented in the electric equivalent circuit with the constant phase element (CPE)[47]. CPE impedance Z_{CPE} is definable as $[Q(j\omega)]^{-\alpha}$, where Q is heterogeneous quasi-capacitance in case of frequency dispersion effects and CPE exponent α is the so-called homogeneity factor (for α=1 CPE represents ideal capacitor) [47]. Since the diffusion tail was not present in the vast majority of studied cases, the Z_W was excluded from the electric equivalent circuit. In order to do so, authors restricted the low-frequency range used (to 100 mHz) for the analysis of impedance spectra recorded for the reference sample as well as worst performing inhibitor (**3**). We found it to be the best alternative for a reliable corrosion inhibitory action comparison using one fitting model for each case scenario. The goodness fit, represented by the chi^2 parameter was ranging between $5.0*10^{-4}$ and $2.3*10^{-3}$.

Fig. 7 presents the dependence of various impedance parameters derived from the equivalent circuit as a function of the corrosion inhibitor concentration. Fitting results are also shown in **Table S1**, **Supporting Information**). For each studied corrosion inhibitor, the values of R_{ct} increase with concentration, demonstrating a delayed corrosion process (**Fig. 7a**). The R_{ct} also allowed to calculate the inhibition efficiency using eq. (1) derivative, IE = (1- R_{ct}^0/R_{ct}) *100% [47], which is plotted in **Fig. 7b**. The highest corrosion inhibition efficiency is offered by inhibitor (5), followed by inhibitor (4). At the same time, these are the only two studied molecules to offer satisfactory inhibition efficiency exceeding 90%, even at low concentrations of ~0.1 mM.

The quasi-capacitance represents the cumulative effect of the heterogeneous corrosion inhibitor film and the electric double layer. Its value tends to decrease with inhibitor concentration (see **Fig. 7c**) as a result of a decrease in the local dielectric constant (s) and/or rise in the electrical double layer thickness (d) [48]. This affirms the adsorption of inhibitor molecules and subsequent film formation, which hinders the diffusion of Cu^{2+} from the Cu/solution interface to the solution thus, diminishing the dissolution reactions (corrosion) of copper [49]. The homogeneity factor α plotted in the inset of **Fig. 7c** reveals that the frequency dispersion effect is the least prominent in case of film formed by inhibitor (**5**) molecules. This effect should be connected with the highest surface coverage and homogeneity of adsorbed film, as well as stationary conditions obtained due to the reduced corrosion rate, corroborating previous findings.

3.3. Characterizations of the corroded and inhibited Cu surfaces

3.3.1. High-resolution XPS results

The XPS studies were conducted on the corroded and inhibited Cu samples pre-exposed in electrolytic conditions for 8h to examine the interaction of studied corrosion inhibitor molecules with the corrosion products on copper surface. A freshly polished Cu sample was also examined for the reference purposes. The analyses were carried out in the binding energy (BE) range of *Cu2p*, *O1s*, *C1s* and *N1s* peaks. The acquired XPS spectra are presented together with proposed peak deconvolution in **Fig. 8**.

The $Cu2p_{3/2}$ spectra of the polished sample (reference) reveals only single spectral component, naturally characteristic for metallic Cu. Its location at 932.8 eVis in good agreement with the literature data [50]. The surface chemistry of copper sample is strongly altered as a result of pre-exposure in the alkaline electrolyte, resulting in the appearance of two additional components, corresponding to copper corrosion products (Cu(II) oxides; BE at 934.0 *eV* and Cu(II) carbonate dihydroxide; BE at 935.6 *eV* [51]. The presence of these compounds corroborates the Pourbaix diagrams of copper in alkaline media, while CuO presence may be further confirmed through strong satellite feature observed at higher energy range, approx. 940-945 *eV*. The signal from metallic copper is still present in the case of corroded sample, yet its share is much smaller (10% of total copper). Thus, this feature may be one of the indicators of copper oxidation kinetics in alkaline electrolyte. Comparison of the inhibition efficiencies offered by studied compounds reveals that only in the presence of inhibitor **(5)**, Cu surface oxidation rate is negligible and Cu^0 share is 87% of all copper components. In the case of inhibitors **(3)**, **(4)** and **(6)** the resultant Cu^0 shares are 43%, 26% and 20%, respectively. The Cu corrosion may be confirmed through the strong +1.2 *eV* peak shift and prominent Cu(II) satellite feature. The $Cu2p_{3/2}$ main signal-to-satellite peak ratio registered for **(4)** and **(6)** compounds was very similar, equal to 2.6:1 and 2.8:1,

respectively. This ratio is significantly higher for **(3)** compound (3.9:1), testifying weaker Cu(II) contribution in this case. On the other hand, the Cu(II) satellite feature was negligible in the case of (5) compounds owing to the highest corrosion inhibition efficiency.

It is also worth to note that the strengths of signals originating from various Cu forms are the weakest for samples **(3)** and **(5)**, indicating the formation of an adsorbed film of the inhibitor molecules and corroborating hindered surface oxidation. The analyses carried out for spectra recorded in *O1s*, *C1s* and *N1s* BE range confirm the previously drawn conclusions. The *O1s* signal may be deconvoluted into three various components, depending on the studied material. In the case of polished electrode, only small contribution from oxygen and carbon is present(<7 at.%), location characteristic for adventitious carbon contamination [52].

On the other hand, spectra recorded for samples pre-exposed in corrosive media differ significantly. The *O1s* signal intensifies and two major components may be recognized: at approx. 529.9 *eV*, an energy characteristic for copper-oxygen bonds and 531.7 *eV*, which should be recognized as copper hydroxides and organic C-O bonds [53-55]. The third and smaller component, located at 532.9 *eV* is primarily associated with carboxylic bonds found in studied inhibitor molecules. The *C1s* peak may be deconvoluted using three spectral components. The energy of the primary component equal to 284.6 *eV* is characteristic to aliphatic C-C bonds resulting from air exposure. Next, two additional components were noted, characteristic to species present within the corrosion products: hydroxyls (at +0.8 *eV*) and carbonates or carboxyls (at +3.0 *eV*) [54, 56].

According to both *O1s* and *C1s* spectral shapes, the interaction of Cu sample with alkaline environment containing compounds **(4)** or **(6)** are essentially alike interaction with electrolyte in absence of corrosion inhibitor. High *O1s* Cu-O signal (13.8 and 11.7 at.%, respectively) testifies the formation of

corrosion product layer and corroborates findings for *Cu2p*$_{3/2}$ spectra. Slightly smaller Cu-O contribution for inhibitor **(3)** (4.8 at.%) is noticed, while its share on the surface of Cu exposed to corrosive media with presence of **(5)** inhibitor is negligible (<1 at.%). These results testify for the increased corrosion resistance offered by the inhibitor compounds **(5)** and **(3)**.

Unlike freely corroded Cu sample, for each sample pre-exposed in electrolyte containing studied inhibitors the *O1s* and *C1s* spectral shape reveal adsorption of the inhibitor molecules on the electrode surface. The difference manifests in the strength of the C-C component, which is more prominent for **(3)** and **(5)** compounds as a result of xanthanese adsorption [57], while in the case of **(4)** and **(6)** inhibitor it is nearly on par with value recorded for freely corroded sample. At the same time small *C1s* shifts are observed due to the appearance of aromatic rings and dehydrogenated sp^3 carbons**.** The contribution of adsorbed xanthene species on the Cu electrode surface of each studied electrode corresponds to corrosion resistance offered by the inhibitor. The intensity of C-O at 285.9 eV increases for each studied compound when compared to sample corroded in absence of inhibitor, which is due to presence of these type of bonds in the synthesized inhibitor molecules. Additionally, the discussed signal is overlapped by the contribution from the cyanide -C≡N bonds at approx. 286 eV [57, 58].

Last but not least, the adsorption of corrosion inhibitor molecules may be confirmed through the appearance of peak on *N1s* spectra, in energy range characteristic for carbon-nitrogen interaction. Interestingly, the *N1s* peaks BE in case of **(4)** and **(6)** inhibitors, C-$N_{(2)}$, are strongly shifted toward more positive energies, characteristic for amides. The C-$N_{(1)}$ interaction for the best performing **(5)** inhibitor is located in the energy range characteristic to cyanides [59]. The detailed chemical analysis is presented in **Table 2**.

3.3.2. Topography studies

The SEM microscopic studies are presented in **Fig. 9a-e**. The micrographs presented for freely corroded Cu sample in the absence of corrosion inhibitor reveal general corrosion, which produces flake-like structures with morphology analogous to this of CuO and $CuCO_3*Cu(OH)_2$[60, 61], see **Fig. 9 (a)**. Similar structures are easily recognized at highest magnifications for samples pre-exposed in presence of inhibitor **(3)**, **(4)** or **(6)**, however in the case of inhibitors **(3)** and **(4)** they possibly agglomerates into larger structures leading to local large crystal formation. The dispersion of barrier properties offered by the adsorbed layer is often found in the case of anodic organic inhibitors, most often due to exceeding of critical inhibition concentration [54]. On the other hand micrographs of Cu sample pre-exposed in **(5)** inhibitor confirm lack of CuO and $CuCO_3*Cu(OH)_2$ corrosion products on the electrode surface. The high efficiency of the corrosion inhibitor is confirmed by negligible corrosion failure. The above presented discussion supports earlier XPS analyses.

3.4. Theoretical studies

3.4.1. Quantum chemical calculations

To examine the correlation between the molecular structure of the four tested inhibitors and their inhibitory characteristics, a quantum chemical analysis was carried out. Frontier molecular orbital theory (FMO), revealed that the chemical reactivity of an inhibitor molecule, in terms of its binding tendency with the metal surface, augments with the augment in the highest occupied molecular orbital (HOMO) and the diminution of the lowest unoccupied molecular orbital (LUMO) energy values, namely E_{HOMO} and E_{LUMO} [62, 63]. The molecule with high (less negative) E_{HOMO} value acts as a good corrosion inhibitor *via* electron donation to unoccupied *d*-orbital of the metal surface, while that with a low (more negative)

E_{LUMO} value possesses an electron accepting ability; both favour inhibitor adsorption resulting in efficient corrosion inhibition [64-66]. This makes the energy gap, $\Delta E = E_{LUMO} - E_{HOMO}$, an important quantum chemical parameter which refers to the inhibitor molecule's reactivity toward adsorption [65, 67]. The lower the ΔE value, the greater is its propensity towards adsorption and hence the higher is its corrosion inhibition efficiency [65, 67]. **Fig. 10** depicts the results of HOMO-LUMO energy values for notr and *solvent phases*.

The E_{HOMO} values for compounds (**3**-**6**) were found to be -5.763, -5.554, -5.517, and -5.723 eV for gas phase and -5.699, -5.496, -5.476 and -5.711 eV for water phase, respectively. The less negative HOMO energy is often explicated by strong adsorption that results in efficient corrosion inhibition. E_{HOMO} values for compounds **3 and 6** are close to each other, referring to their similar charge donating ability to the metallic surface. The same trend can be noticed for **4** and **5**. However, compounds **4** and **5,** with their less negative E_{HOMO} values, are capable of donating electrons to the unoccupied d orbital of the metal, and hence strongly adsorbed, more effectively than **3** and **6** for both gas and water phases. The lower (more negative) E_{LUMO} value calculated for **4** (-3.148 eV), compared with those estimated for **3** (-1.976 eV), **5** (-2.93 eV), and **6** (-2.741 eV) reflects the former's stronger adsorption than the others.

ΔE values of **4**, **5**, **6**, and **3** molecules were found to be 2.406, 2.587, 2.982 and 3.787 eV for the gas phase and 2.571, 2.742, 2.983 and 3.687 eV for the water phase, respectively. Obviously, the xanthene derivatives **4** and **5** exhibited the lowest ΔE values among the molecules tested, indicating their higher capacity to adsorption. Such results support the experimental findings that compounds **4** and **5** are the best in inhibiting the alkaline corrosion of Cu among the other xanthene derivatives studied, **3** and **6**.

FMO is also useful in the prediction of inhibitor molecule adsorption (active) centres, in terms of charge density distribution, responsible for interaction with surface metal atoms [62-66]. In this context,

Fig. 11 is constructed to show the HOMO and LUMO levels' charge density distribution of cyano-benzylidenexanthene derivatives **(3-6)**.

Obviously, the HOMO distributions of molecules are mainly located around the 7*H*-dibenzo[*c,h*]xanthen ring of **(3-6)** molecules, while the LUMO distributions are on the groups attached to the 7*H*-dibenzo[*c,h*]xanthen rings. The electron donating tendencies for the non-protonated forms of the studied inhibitors followed the sequence: **5** > **4** > **6** > **3** for gas phase and **5** > **4** > **3** > **6** for water phase.

According to the Maximum Hardness Principle (MHP), there is a tendency for a chemical system to organize itself to reach maximum hardness, and a measure of stability is the chemical hardness (η) [68]. The inhibitor molecule with a low η value possesses high corrosion inhibition performance [68]. According to chemical hardness values displayed on **Fig. 12**, the corrosion inhibition efficiency ranking of the investigated molecules can be given as: **4** > **5** > **6** > **3** for gas and solvent phases. These findings correspond well to the experimental data obtained.

The chemical softness (σ) is a measure of the polarizability of chemical species. Soft molecules easily donate electrons to metal surface and function as good corrosion inhibitors [69]. Inhibitor adsorption on metal surface takes place through the portion of a molecule that has the highest chemical softness and the lowest hardness [69]. The **(3-6)** compounds' σ values for gas phase were calculated as 0.528, 0.831, 0.773 and 0.671 eV, respectively. This ranks the inhibition efficiency of studied molecules for the gas phase as: **4** > **5** > **6** > **3**. The same sequence of decreasing σ values was achieved for the tested molecules in the water phase (**Fig. 12**). These results are consistent with the experimental findings. According to such calculations, inhibitor **(4)** can be considered as the best corrosion inhibitor, while inhibitor **(3)** was the worst for both notr and water phases.

According to the principle of the equalization of electronegativity, an inhibitor molecule possessing a lower value of χ is correlated with a higher propensity of electron donation and thus exhibited a higher inhibition capacity than the one with a higher χ value [70, 71]. **Fig. 12** reveals that χ values of 3.870, 4.351, 4.224 and 4.232 *eV* in the gas phase, and 3.856, 4.211, 4.105and 4.220 *eV* in the solvent phase are estimated for the inhibitor molecules **(3-6)**, respectively. These results demonstrate that the inhibitor with the least χ value **(3)** is the best inhibitor, while that having the highest χ value **(6)** is the worst.

The high ionization potential (I) values apply to chemical inertness and high stability, while the low ionization potential denotes high atom and molecule activity [72]. The ionization potential values, **Fig. 12**, calculated for inhibitors **3-6** are 5.763, 5.723, 5.554, and 5.517 eV for notr phase, and 5.699, 5.711, 5.496, and 5.476 eV for notr phase, respectively. Based on these calculations, the order of decreasing activity, and hence decreased inhibition efficiency, is: **5** > **4** > **6** > **3** for notr phase, and **5** > **4** > **3** > **6** for water phase.

Dipole moment (DM, Debye) is yet another measure of the corrosion inhibition performance of organic compounds. While some authors claimed that there is no remarkable relationship between dipole moment and inhibition efficiency [63], others revealed that the corrosion inhibitor efficiency increases with increase in the dipole moment, as increased dipole moment expedites electron transfer [73, 74]. This in turn results in firm adsorption, and hence improved inhibition efficiency.For instance, in **Table 3**, the calculated dipole moment values for molecules **(3-6)** are 3.200, 5.674, 3.386 and 3.524, for gas phase, and 3.809, 9.269, 5.009 and 4.542, for water phase, respectively. Here again, based on dipole moment calculations, inhibitor **(4)** is the best corrosion inhibitor for both gas and water phases.

Recently, in corrosion inhibition studies, some authors used global electrophilicity (ω) index of molecules, and they reported that this index is a useful theoretical descriptor in the prediction of inhibitive

performances of molecules against the corrosion of metal surfaces [73, 75]. Parr's index of electrophilicity is based on the molecules' chemical hardness and electronegativity values, as given in Eq. 7 (**Supporting Information**), and nucleophilicity is generally given as the multiplicative inverse of the electrophilicity [76]. It is apparent that molecules having high electrophilicity values are ineffective to prevent metal corrosion. A good corrosion inhibitor should therefore possess low electrophilicity or high nucleophilicity values [76]. Considering the values of ω presented in **Table 3**, inhibitor **3** can be considered as the best one among studied inhibitors in both gas and water phases, as it recorded the lowest ω value amongst.

The results of other quantum chemical calculations, namely the total of negative Mulliken atomic charges (*TMAC*), Chemical potential (μ) and molar volume (*MV*) can be seen in **Table 3**. The higher negative value of TMAC favors inhibitor adsorption [77]. According to TMAC results presented in **Table 3**, the inhibitor **(6)** is expected to be the best corrosion inhibitor for gas and water phases.

The more reactive nucleophile features a lower (μ) value, as it measures the propensity of chemical species to accept electrons [77]. As shown in **Table 3**, the lowest (μ) value (-4.351 and -4.220 eV for the gas and water phases, respectively) was recorded for the inhibitor **(4)**, as the best corrosion inhibitor among group members for gas and water phases.

It is commonly accepted that the molecular volume (MV) is a measure for the possible metal surface coverage by the inhibitor [77]. It expresses the contact surface between the adsorbed molecule and metal surface. The compound with a large (*MV*) value is expected to efficiently protect metal surface against corrosion, as the efficacy of the corrosion inhibition is generally proportional to the fraction of the surface covered by the molecule of the adsorbed inhibitor [77]. Based on (*MV*) values, for the gas phase, the order of decreasing inhibition efficiency can be written as: **5** > **6** > **4** > **3**. This order is disturbed for

the water phase; the inhibition performance of the studied organic molecules is found to decrease following the sequence: **6** > **4** > **5** > **3**.

The compound's electrostatic potential (ESP) distribution, one of the essential tools to study the compounds' reactivity nature as it measures their electrophilic and nucleophilic nature, can be precisely studied by the DFT approach [67]. The ESP graphs' blue colour refers to the maximum amount of the positive region where the nucleophilic reaction can occur, while its reddish region points to the negative region where preferential electrophilic reactions occur [67]. The molecule's electron-rich regions are the most active. Different colours represent different values of the electrostatic potential surface of the compounds, and the ESP increases following the sequence: red < orange < yellow < green < blue.

It follows from **Fig. 13** that the electron density concentrations around the oxygen atom for molecule **(3)**, and nitrogen and oxygen atoms for **(4-6)** molecules for notr and water phases. This result reveals that the molecules preferentially adsorb *via* their oxygen and nitrogen atoms. Especially, most of the electrophilic reactions take place through O30 for **(3)** and O34, O35 and N32 atoms for **4**, **5** and **6** molecules, and the red coloured regions in **Fig. 13** show the maximum electronegativity.

Electronic charging analysis of atoms in the molecules is essential to evaluate their corrosion inhibition efficiency, since a molecule's binding capability, and hence its adsorption capacity and subsequent effective corrosion inhibition, relies on the electronic charge on the heteroatoms of that molecule [60]. In this context, Mulliken population analysis [73] has been used to calculate the Mulliken negative atomic charges on the oxygen and nitrogen atoms of the investigated inhibitor molecules, **Table 4**. It is obvious that the molecules' Mulliken negative atomic charges are more in the vicinity of the O30 atom for inhibitor **(3)** molecule, and N32, O34 and O35 atoms for other molecules. Binding the molecule from these atoms is easier, since the negative value is higher. Increasing the negative load values

on these atoms is therefore expected to cause efficient corrosion inhibition as a simple consequence of effective adsorption.

4. Conclusions

Four novel xanthene derivatives **(3-6)** were successfully prepared, fully characterized and further investigated as inhibitors for the corrosion of Cu in alkaline solutions. Measurements were performed in 1.0 M NaOH without and with different concentrations (ca. 0.1-1.0 mM) of the inhibitors examined using various electrochemical techniques. The efficiency of each studied inhibitor towards the alkaline corrosion of Cu was found to enhance with inhibitor concentration, reaching its maximum value (91.8, 94.4, 97.2, and 98.7% for **3**, **6**, **4**, and **5**, respectively) at a concentration of 1.0 mM. Our newly synthesized xanthenes' inhibition efficiency values, particularly those recorded for compounds **5** (98.7%) and **4** (97.2%) at 1.0 mM inhibitor concentration, surpassed that exhibited by methionine (90.8% @ 10 mM inhibitor concentration) for copper corrosion in 1.0 M NaOH solution [46], and many others reported in the literature for the corrosion of copper under alkaline conditions [29,30]. Polarization measurements demonstrated that the four synthesized xanthenes acted as mixed-type inhibitors for the alkaline copper corrosion. Adsorption of the inhibitor molecules and subsequent development of a protective film was confirmed from XPS study. Surface topography of the corroded and inhibited Cu surfaces showed that the corroded areas on the electrode surface were efficiently diminished in presence of inhibitor **5**. Full computational studies were also performed on the synthesized xanthene derivatives **(3-6)** in order to corroborate experimental findings. The various quantum chemical parameters, estimated using Gaussian 09 (Revision A.02) software with B3LYP/6-311G(d,p) basic set for both gas and water phases, such as frontier orbital energies, energy gap, ionization energy, chemical hardness, softness, dipole moment, electronegativity, electrophilicity, nucleophilicity, Mulliken charges, revealed that the corrosion inhibitor efficiency for gas and water phases can be ranked as: **4** > **5** > **6** > **3**. Theoretical data were found

to agree largely with the experimental findings. In a continuation of this work, with the objective to effectively mitigate copper corrosion under severe conditions, our coming research plan of work will focus on developing new thin films (as corrosion protective smart coatings) based on M NPs (M = Co, Ni, and Ag) supported on highly defective monoclinic hydroxyl-functionalized ZrO_2 nanoparticles with high surface area, prepared by a sol-gel method with Chitosan as nano-assembling template.

References

[1] R.d.P.B. Hernández, I.V. Aoki, B. Tribollet, H.G. de Melo, Electrochemical impedance spectroscopy investigation of the electrochemical behaviour of copper coated with artificial patina layers and submitted to wet and dry cycles,Electrochim. Acta56 (2011) 2801-2814.
[2] B. Duran, G. Bereket, M. Duran,Electrochemical synthesis and characterization of poly(m-phenylenediamine) films on copper for corrosion protection, Prog. Org. Coat.73 (2012) 162-168.
[3] E.-S.M. Sherif, R.M. Erasmus, J.D. Comins,Corrosion of copper in aerated acidic pickling solutions and its inhibition by 3-amino-1,2,4-triazole-5-thiol, J. Colloid Interface Sci.306 (2007) 96-104.
[4] S.B. Adeloju, H.C. Hughes,The corrosion of copper pipes in high chloride-low carbonate mains water, Corros. Sci.26 (1986) 851-870.
[5] T. Suter, E.M. Moser, H. Böhni, The characterization of the tarnishing of Cu-15Ni-8Sn and Cu-5Al-5Sn alloys,Corros. Sci.34 (1993) 1111-1122.
[6] K. Habib, In-situ monitoring of pitting corrosion of copper alloys by holographic interferometry, Corros. Sci.40 (1998) 1435-1440.
[7] R.M. Souto, M.P. Sánchez, M. Barrera, S. González, R.C. Salvarezza, A.J. Arvia,The kinetics of pitting corrosion of copper in alkaline solutions containing sodium perchlorate,Electrochim. Acta37 (1992) 1437-1443.
[8] A.A. Attia, E.M. Elmelegy, M. El-Batouti, A.M. Ahmed,Anodic Corrosion Inhibition in Presence of Protic Solvents, Asian J. Chem.28 (2016) 267-272.
[9] B. Tan,S. Zhang,Y. Qiang,L. Guo,S. Chen,A combined experimental and theoretical study of the inhibition effect of three disulfide-based flavouring agents for copper corrosion in 0.5 M sulfuric acid, J. Colloid Interface Sci.52615 (2018) 268-280.
[10] S. Mo,H.Q. Luo,N.B. Li, Study on the influences of two thiazole flavor ingredients on Cu corrosion caused by chloride ion, J. Colloid Interface Sci.5051 (2017) 929-939.
[11] Y. Qiang,S. Zhang,S. Xu,W. Li, Experimental and theoretical studies on the corrosion inhibition of copper by two indazole derivatives in 3.0% NaCl solution, J. Colloid Interface Sci.47215 (2016) 52-59.
[12] El-Sayed M. Sherif,R.M. Erasmus,J.D. Comins,Corrosion of copper in aerated synthetic sea water solutions and its inhibition by 3-amino-1,2,4-triazole, J. Colloid Interface Sci.309 (2007) 470-477.

[13] El-Sayed M. Sherif,R.M. Erasmus,J.D. Comins, Effects of 3-amino-1,2,4-triazole on the inhibition of copper corrosion in acidic chloride solutions, J. Colloid Interface Sci.311 (2007) 144-151.
[14] K.F. Khaled, M.A. Amin, Dry and wet lab studies for some benzotriazole derivatives as possible corrosion inhibitors for copper in 1.0 M HNO_3, Corros. Sci.51 (2009) 2098-2106.
[15] K.F. Khaled, M.A. Amin,N.A. Al-Mobarak,On the corrosion inhibition and adsorption behaviour of some benzotriazole derivatives during copper corrosion in nitric acid solutions: a combined experimental and theoretical study,J. Appl. Electrochem,40 (2010) 601-613.
[16] W. Qafsaoui, M.W. Kendig, H. Takenouti, F. Huet, Corrosion Inhibition of Copper by Selected Thiol Compounds, ECS Trans.13 (2008) 123-132.
[17] F. Caprioli, F. Decker, A.G. Marrani, M. Beccari, V.D. Castro,Copper protection by self-assembled monolayers of aromatic thiols in alkaline solutions, Phys. Chem. Chem. Phys.12 (2010) 9230-9238.
[18] G.L.F. Mendonça, S.N. Costa, V.N. Freire, P.N.S. Casciano, A.N. Correia, P.d. Lima-Neto, Understanding the corrosion inhibition of carbon steel and copper in sulphuric acid medium by amino acids using electrochemical techniques allied to molecular modelling methods, Corros. Sci.115 (2017) 41-55.
[19] B. El Ibrahimi, A. Jmiai, L. Bazzi, S. El Issami, Amino acids and their derivatives as corrosion inhibitors for metals and alloys, Arab J. Chem.13 (2020) 740-771.
[20] M.A. Amin, K.F. Khaled,Copper corrosion inhibition in O_2-saturated H_2SO_4 solutions,Corros. Sci. 52 (2010) 1194-1204.
[21] Y. Yu, D. Zhang, H. Zeng, B. Xie, L. Gao, T. Lin, Synergistic effects of sodium lauroyl sarcosinate and glutamic acid in inhibition assembly against copper corrosion in acidic solution, Appl. Surf. Sci.355 (2015) 1229-1237.
[22] H. Ma, S. Chen, B. Yin, S. Zhao, X. Liu,Impedance spectroscopic study of corrosion inhibition of copper by surfactants in the acidic solutions,Corros. Sci. 45 (2003) 867-882.
[23] S. Ullah, A.M. Shariff, M. A.Bustam, M. Nadeem, M.Y. Naz, M. Ayoub,Study on Effect of Benzotriazole and Surfactants on Corrosion Inhibition of Copper Alloys in Sulphuric Acid, Int. J. Electrochem. Sci.10 (2015) 8321-8333.
[24] K. Cao, H.Y. Sun, B.R. Hou,Corrosion Inhibition of Gemini Surfactant for Copper in 3.5% NaCl, Adv. Mater. Res. 936 (2014) 1125-1131.
[25] M.A. Amin, Weight loss, polarization, electrochemical impedance spectroscopy, SEM and EDX studies of the corrosion inhibition of copper in aerated NaCl solutions, J. Appl. Electrochem.36 (2006) 215-226.
[26] T. Notoya, V. Otieno-Alego, D.P. Schweinsberg, The corrosion and polarization behaviour of copper in domestic water in the presence of Ca, Mg and Na-Salts of phytic acid,Corros. Sci. 37 (1995) 55-65.
[27] H. Yang, Y. Yang, Y. Yang, H. Liu, Z. Zhang, G. Shen, R. Yu, Formation of inositol hexaphosphate monolayers at the copper surface from a Na-salt of phytic acid solution studied by in situ surface enhanced Raman scattering spectroscopy, Raman mapping and polarization measurement, Anal. Chim. Acta548 (2005) 159-165.

[28] Y.-H. Wang, J.-B. He, Corrosion inhibition of copper by sodium phytate in NaOH solution: Cyclic voltabsorptometry for in situ monitoring of soluble corrosion products,Electrochim. Acta66 (2012) 45-51.
[29] A. Fateh, M. Aliofkhazraei, A.R. Rezvanian, Review of corrosive environments for copper and its corrosion inhibitors, Arab J. Chem. 13 (2020) 481-544.
[30] M.M. Antonijevic, M.B. Petrovic,Copper Corrosion Inhibitors. A review, Int. J. Electrochem. Sci.3 (2008) 1-28.
[31] J.R. Dimmock, S.K. Raghavan, G.E. Bigam,Evaluation of Mannich bases of 2-arylidene-1,3-diketones versus murine P388 leukemia, Eur. J. Med. Chem.23 (1988) 111-117.
[32] S. Samantaray, P. Kar, G. Hota, B.G. Mishra,Sulfate Grafted Iron Stabilized Zirconia Nanoparticles as Efficient Heterogenous Catalysts for Solvent-Free Synthesis of Xanthenediones under Microwave Irradiation, Ind. Eng. Chem. Res. 52 (2013) 5862-5870.
[33] H.-K. Wang, S.L. Morris-Natschke, K.-H. Lee,Recent advances in the discovery and development of topoisomerase inhibitors as antitumor agents,Med. Res. Rev. 17 (1997) 367-425.
[34] A.V. Rukavishnikov, M.P. Smith, G. Bruce Birrell, J.F.W. Keana, O. Hayes Griffith,Synthesis of a new fluorogenic substrate for the assay of phosphoinositide-specific phospholipase C, Tetrahedron Lett.39 (1998) 6637-6640.
[35] N.O. Obi-Egbedi, I.B. Obot, Adsorption behavior and corrosion inhibitive potential of xanthene on mild steel/sulphuric acid interface, Arab J. Chem.5 (2012) 121-133.
[36] N.O. Obi-Egbedi, I.B. Obot, A new and effective corrosion inhibitor for mild steel in sulphuric acid solution, Arab J. Chem.6 (2013) 211-223.
[37] B. Maleki, A. Davoodi, M.V. Azghandi, M. Baghayeri, E. Akbarzadeh, H. Veisi, S.S. Ashrafi, M. Raei, Facile synthesis and investigation of 1,8-dioxooctahydroxanthene derivatives as corrosion inhibitors for mild steel in hydrochloric acid solution, New J. Chem.40 (2016) 1278-1286.
[38] C. Verma, J. Haque, M.A. Quraishi, E.E. Ebenso, Aqueous phase environmental friendly organic corrosion inhibitors derived from one step multicomponent reactions: A review, J. Mol. Liq. 2751 (2019) 18-40.
[39] M.E. Khalifa, A.A. Gobouri, F.M. Kabli, T.A. Altalhi, A.S.A. Almalki, M.A. Mohamed, Antibacterial, and Anti HepG2 Cell Line Human Hepatocyte Carcinoma Activity of Some New Potentially Benzimidazole-5-(Aryldiazenyl)Thiazole Derivatives, Molecules23 (2018) 3285.
[40] B.V. Appa Rao, M.Y. Iqbal, B. Sreedhar, Electrochemical and surface analytical studies of the self-assembled monolayer of 5-methoxy-2-(octadecylthio)benzimidazole in corrosion protection of copper,Electrochim. Acta55 (2010) 620-631.
[41] J. Pople, M. Frisch, G. Trucks, H. Schlegel, G. Scuseria, Gaussian, Inc., Wallingford CT, 2004 Gaussian 03W (Revision C. 01), Gaussian. Inc., Wallingford CT 2003.
[42] N.D. Kokare, J.N. Sangshetti, D.B. Shinde, Oxalic acid as a catalyst for efficient synthesis of bis-(indolyl) methanes, and 14-aryl-14H-dibenzo [a, j] xanthenes in water, Chin. Chem. Lett.19 (2008) 1186-1189.

[43] C.C. Cariou, G.J. Clarkson, M. Shipman,Rapid synthesis of 1,3,4,4-tetrasubstituted beta-lactams from methyleneaziridines using a four-component reaction, J Org.Chem.73 (2008) 9762-9764.

[44] M.A. Amin, K.F. Khaled, S.A. Fadl-Allah, Testing validity of the Tafel extrapolation method for monitoring corrosion of cold rolled steel in HCl solutions–experimental and theoretical studies,Corros. Sci. 52 (2010) 140-151.

[45] Y. Qiang, S. Zhang, S. Xu, L.Yin, The effect of 5-nitroindazole as an inhibitor for the corrosion of copper in a 3.0% NaCl solution, RSC Adv. 5 (2015) 63866-63873.

[46] J. Wu, X. Zheng, W. Li, L. Yin, S. Zhang, Copper corrosion inhibition by combined effect of inhibitor and passive film in alkaline solution, Res Chem Intermed 41 (2015) 8557–8570.

[47] J. Wysocka, M. Cieslik, S. Krakowiak, J. Ryl, Carboxylic acids as efficient corrosion inhibitors of aluminium alloys in alkaline media, Electrochim Acta, 289 (2018) 175-192.

[48] E. McCafferty, N. Hackerman, Double layer capacitance of iron and corrosion inhibition with polymethylene diamines,J. Electrochem. Soc. 119 (1972) 146.

[49] S. Pareek, D. Jain, S. Hussain, A. Biswas, R. Shrivastava, S.K. Parida, H.K. Kisan, H. Lgaz, I.-M. Chung, D. Behera, A new insight into corrosion inhibition mechanism of copper in aerated 3.5 wt.% NaCl solution by eco-friendly Imidazopyrimidine Dye: experimental and theoretical approach,Chem. Eng. J. 358 (2019) 725-742.

[50] M.C. Biesinger, L.W.M. Lau, A.R. Gerson, R.S.C. Smart, Resolving surface chemical states in XPS analysis of first row transition metals, oxides and hydroxides: Sc, Ti, V, Cu and Zn, Appl. Surf. Sci. 257 (2010) 887-898.

[51] F.A. Akgul, G. Akgul, N. Yildirim, H.E. Unalan, R. Turan, Influence of thermal annealing on microstructural, morphological, optical properties and surface electronic structure of copper oxide thin films. Mater. Chem. Phys. 147 (2014) 987-995.

[52] M.A. Baker, P. Hammer, Study of the Chemical Composition and Microstructure of Ion Beam-deposited CNx Films Including an XPS C 1s Peak Simulation, Surf. Interface Anal. 25 (1997)629-642.

[53] J. Zhang, Z. Liu, G.-C. Han, S.-L. Chen, Z. Chen, Inhibition of copper corrosion by the formation of Schiff base self-assembled monolayers, Appl. Surf. Sci. 389 (2016) 601-608.

[54] J. Wysocka, S. Krakowiak, J. Ryl, Evaluation of citric acid corrosion inhibition efficiency and passivation kinetics for aluminium alloys in alkaline media by means of dynamic impedance monitoring, Electrochim. Acta 258 (2017) 1463-1475.

[55] E. Cano, C.L. Torres, J.M. Bastidas, An XPS study of copper corrosion originated by formic acid vapour at 40% and 80% relative humidity,Mater. Corros. 52 (2001) 667-676.

[56] J. Ryl, J. Wysocka, M. Cieslik, H. Gerengi, T. Ossowski, S. Krakowiak, P. Niedzialkowski, Understanding the origin of high corrosion inhibition efficiency of bee products towards aluminium alloys in alkaline environments,Electrochim. Acta 304 (2019) 263-274.

[57] S. Fleutot, J.-C. Dupin, G. Renaudin, H. Martinez, Intercalation and grafting of benzene derivatives into zinc–aluminum and copper–chromium layered double hydroxide hosts: an XPS monitoring study, Phys. Chem. Chem. Phys. 13 (2011) 17564-17578.

[58] L. Yang, F. Jia, B. Yang, S. Song, Efficient adsorption of $Au(CN)^{2-}$ from gold cyanidation with graphene oxide-polyethylenimine hydrogel as adsorbent, Results in Physics 7 (2017) 4089-4095.

[59] J.R. Rumble Jr.,D.M. Bickham, C.J. Powell, The NIST x-ray photoelectron spectroscopy database, Surf.Interface Anal.19 (1992) 241-246.
[60] F. Xiao, S. Yuan, B. Liang, G. Li, S.O. Pehkonen, T. Zhang, Superhydrophobic CuO nanoneedle-covered copper surfaces for anticorrosion, J. Mater. Chem. A 3 (2015) 4374-4388.
[61] M.M. Mennucci, M. Sanchez-Moreno, I.V. Aoki, M-C. Bernard, H.G. de Melo, S. Joiret, V. Vivier, Local electrochemical investigation of copper patina. J Solid State Electrochem 16 (2012) 109–116.
[62] M. Djenane, S. Chafaa, N. Chafai, R. Kerkour, A. Hellal, Synthesis, spectral properties and corrosion inhibition efficiency of new ethyl hydrogen [(methoxyphenyl) (methylamino) methyl] phosphonate derivatives: Experimental and theoretical investigation. J. Mol. Struct. 2019,1175, 398-413.
[63] R. Yıldız, An electrochemical and theoretical evaluation of 4,6-diamino-2-pyrimidinethiol as a corrosion inhibitor for mild steel in HCl solutions, Corros. Sci. 2015,90, 544-553.
[64]G. Gece, S. Bilgiç, Quantum chemical study of some cyclic nitrogen compounds as corrosion inhibitors of steel in NaCl media, Corro. Sci. 51 (2009) 1876-1878.
[65]J. Bhawsar, P. Jain, M.G. Valladares-Cisneros, C. Cuevas-Arteaga, M.R. Bhawsar, Quantum chemical assessment of two natural compounds: Vasicine and Vasicinone as green corrosion inhibitors, Int. J. Electrochem. Sci. 13(2018) 3200-3209.
[66] D. Bhattacharjee, T.K. Devi, R. Dabrowski, A. Bhattacharjee, Birefringence, polarizability order parameters and DFT calculations in the nematic phase of two bent-core liquid crystals and their correlation, J. Mol. Liq. 272 (2018) 239-252.
[67] R.G. Parr, P.K. Chattaraj, Principle of maximum hardness, J. Am. Chem. Soc.113 (1991) 1854-1855.
[68] L. Guo, S. Zhu, S. Zhang, Q. He, W. Li, Theoretical studies of three triazole derivatives as corrosion inhibitors for mild steel in acidic medium, Corros. Sci. 87 (2014) 366-375.
[69] R. Hasanov, M. Sadıkoğlu, S. Bilgiç, Electrochemical and quantum chemical studies of some Schiff bases on the corrosion of steel in H_2SO_4 solution, Appl. Surf. Sci. 253 (2007) 3913-3921.
[70] G. van Hooydonk, Z. Eeckhaut, On the Principle of Electronegativity Equalization and its Use in the Theory of the Chemical Bond, Berichte der Bunsengesellschaft für physikalische Chemie 74 (1970) 323-326.
[71] C. Verma, M.A. Quraishi, K. Kluza, M. Makowska-Janusik, L.O. Olasunkanmi, E.E. Ebenso, Corrosion inhibition of mild steel in 1M HCl by D-glucose derivatives of dihydropyrido [2,3-d:6,5-d′] dipyrimidine-2, 4, 6, 8(1H,3H, 5H,7H)-tetraone, Sci. Rep. 7 (2017) 44432.
[72] J. Bhawsar, P. Jain, M.G. Valladares-Cisneros, C. Cuevas-Arteaga, M.R. Bhawsar, Quantum Chemical Assessment of Two Natural Compounds: Vasicine and Vasicinone as Green Corrosion Inhibitors, Int. J. Electrochem. Sci. 13 (2018) 3200-3209.
[73] G. Gao, C. Liang, Electrochemical and DFT studies of β-amino-alcohols as corrosion inhibitors for brass,Electrochim. Acta 52 (2007) 4554-4559.
[74] M. Şahin, G. Gece, F. Karcı, S. Bilgiç, Experimental and theoretical study of the effect of some heterocyclic compounds on the corrosion of low carbon steel in 3.5% NaCl medium, J. Appl. Electrochem. 38 (2008) 809-815.

[75]M.A. Quraishi, R. Sardar, Hector bases – a new class of heterocyclic corrosion inhibitors for mild steel in acid solutions, J. Appl. Electrochem. 33 (2003) 1163-1168.
[76] A. Tazouti, M. Galai, R. Touir, M.E. Touhami, A. Zarrouk, Y. Ramli, M. Saraçoğlu, S. Kaya, F. Kandemirli, C. Kaya, Experimental and theoretical studies for mild steel corrosion inhibition in 1.0M HCl by three new quinoxalinone derivatives, J. Mol. Liquids 221 (2016), 815-832.
[77] M. Shahraki, M. Dehdab, S. Elmi, Theoretical studies on the corrosion inhibition performance of three amine derivatives on carbon steel: Molecular dynamics simulation and density functional theory approaches, J. Taiwan Instit. Chem. Eng.62 (2016) 313-321.

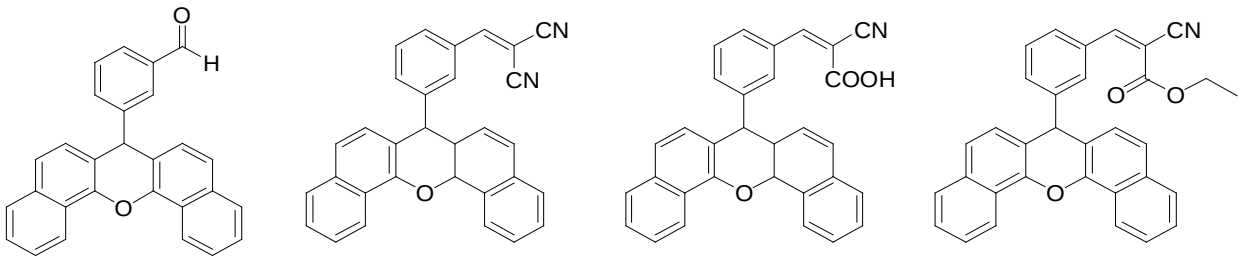

3 **4** **5** **6**

Figure 1. Chemical structures of the four synthesized cyano-benzylidene xanthene derivatives **(3-6).**

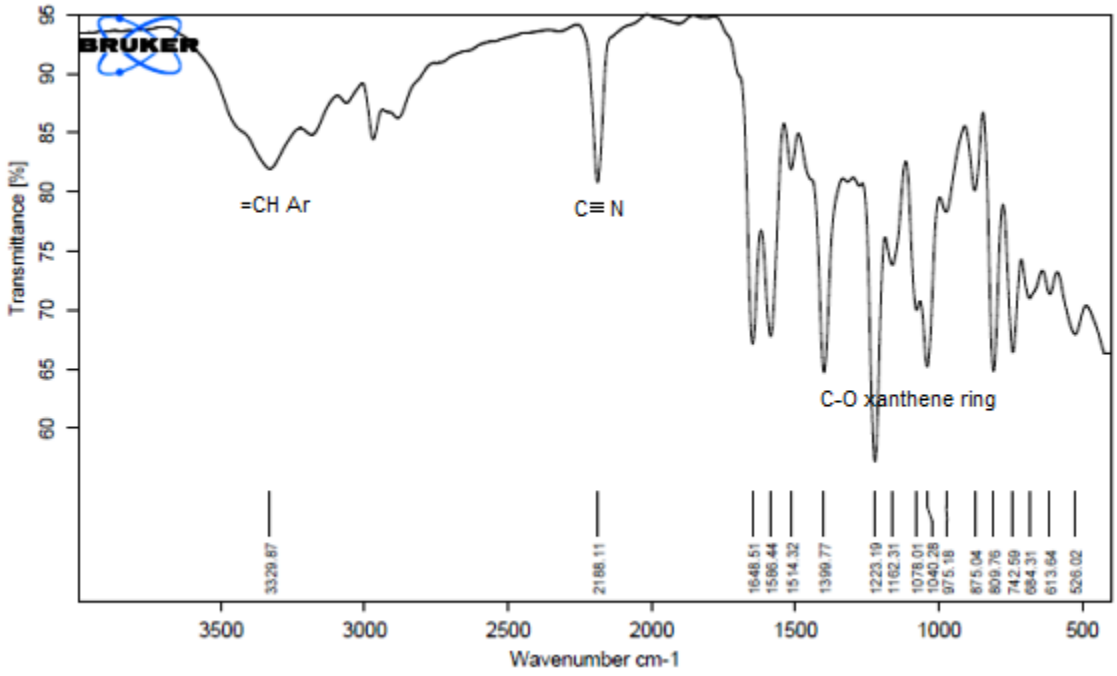

Figure 2a. IR spectra of 2-(3-(7H-dibenzo[*c*,*h*]xanthen-7-yl)benzylidene)malononitrile **(4)**

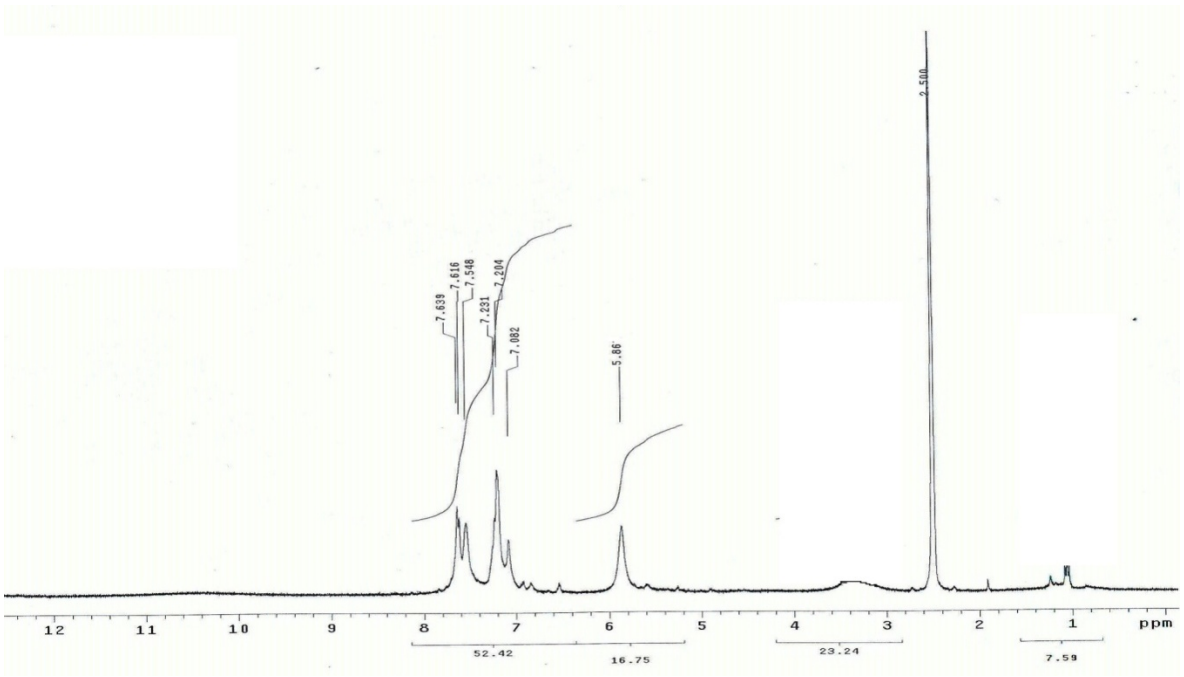

Figure 2b. [1]H NMR spectra of 2-(3-(7*H*-dibenzo[*c*,*h*]xanthen-7-yl)benzylidene)malononitrile **(4)**

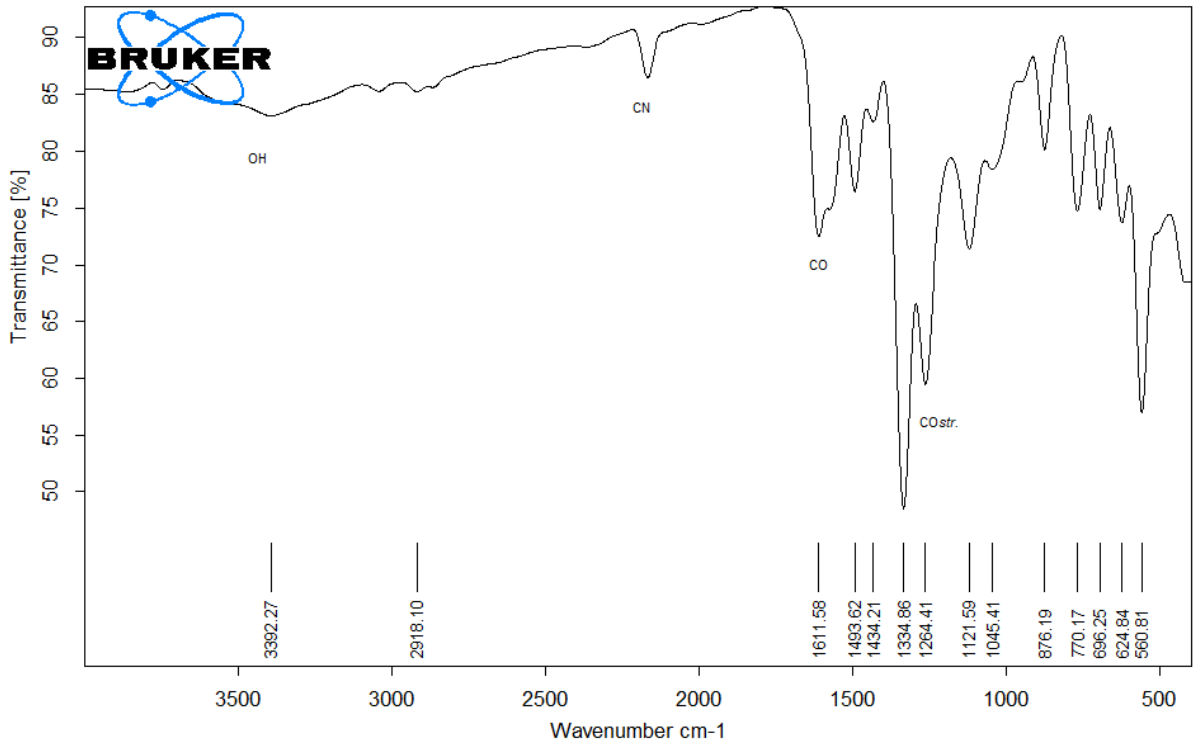

Figure 3a. IR spectra of 3-(3-(7*H*-dibenzo[*c*,*h*]xanthen-7-yl)phenyl)-2-cyanoacrylic acid **(5)**

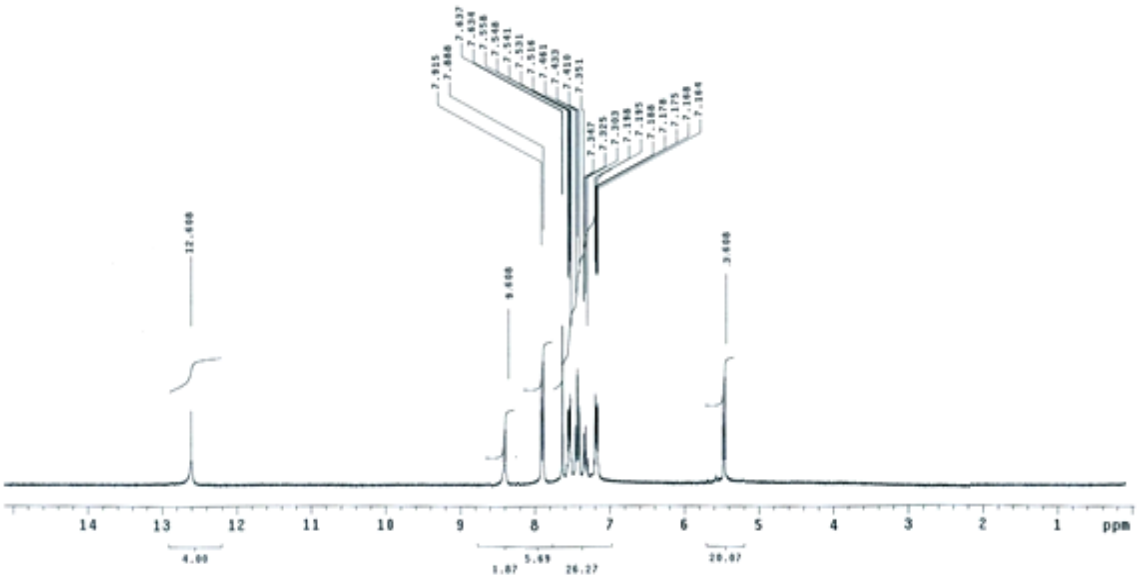

Figure 3b. [1]H NMR spectra of 3-(3-(7*H*-dibenzo[*c*,*h*]xanthen-7-yl)phenyl)-2-cyanoacrylic acid **(5)**

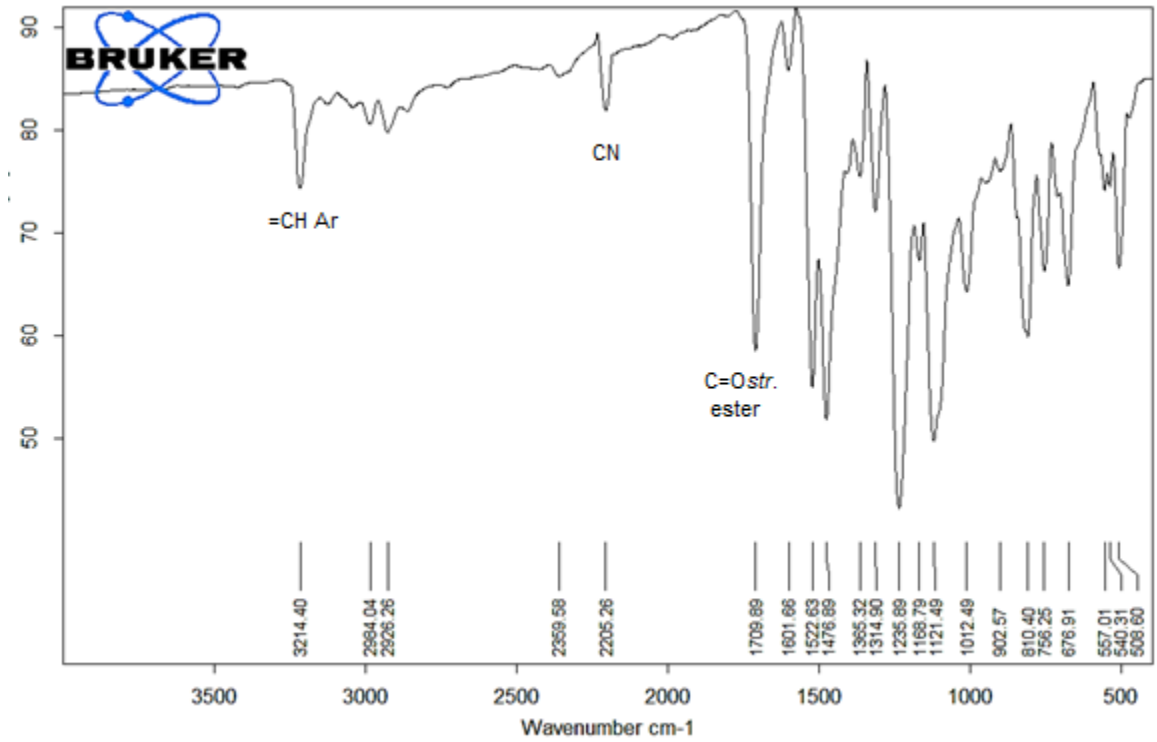

Figure 4a. IR spectra of ethyl-3-(3-(7*H*-dibenzo[*c*,*h*]xanthen-7-yl)phenyl)-2-cyanoacrylate **(6)**

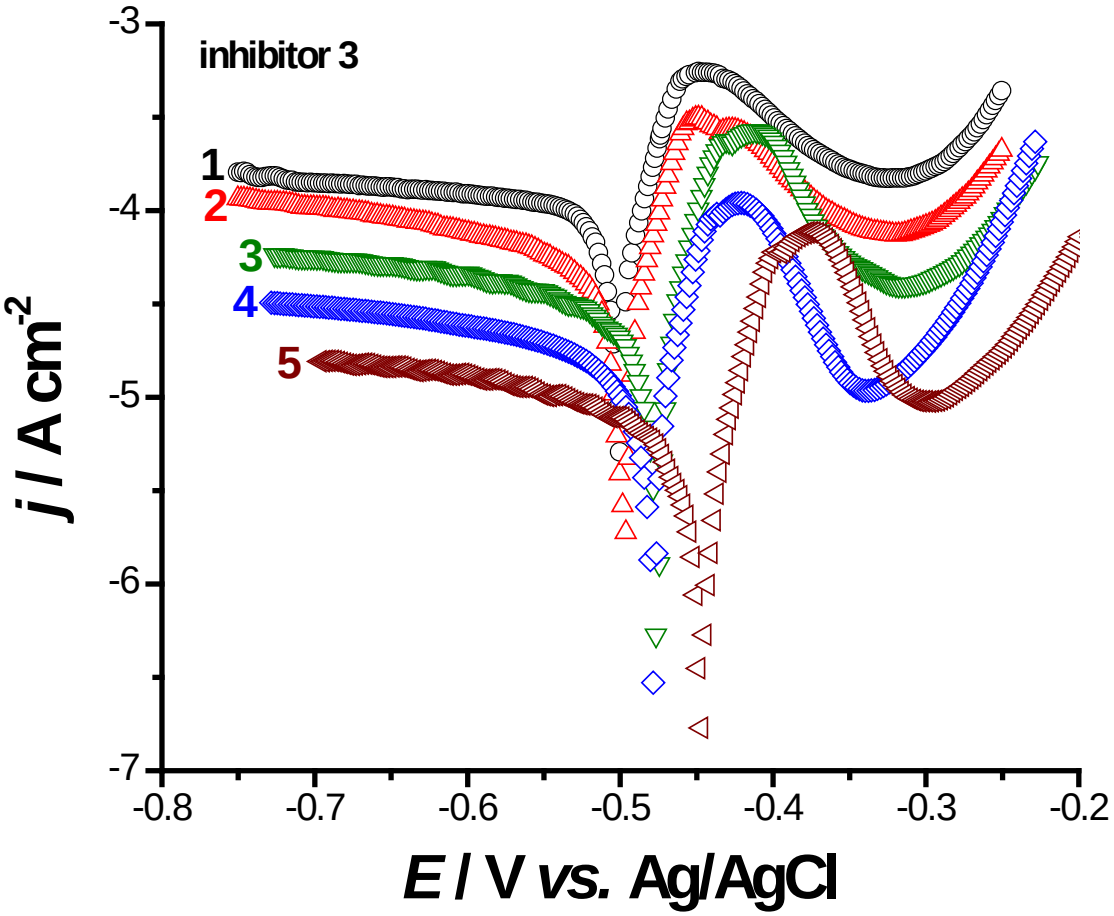

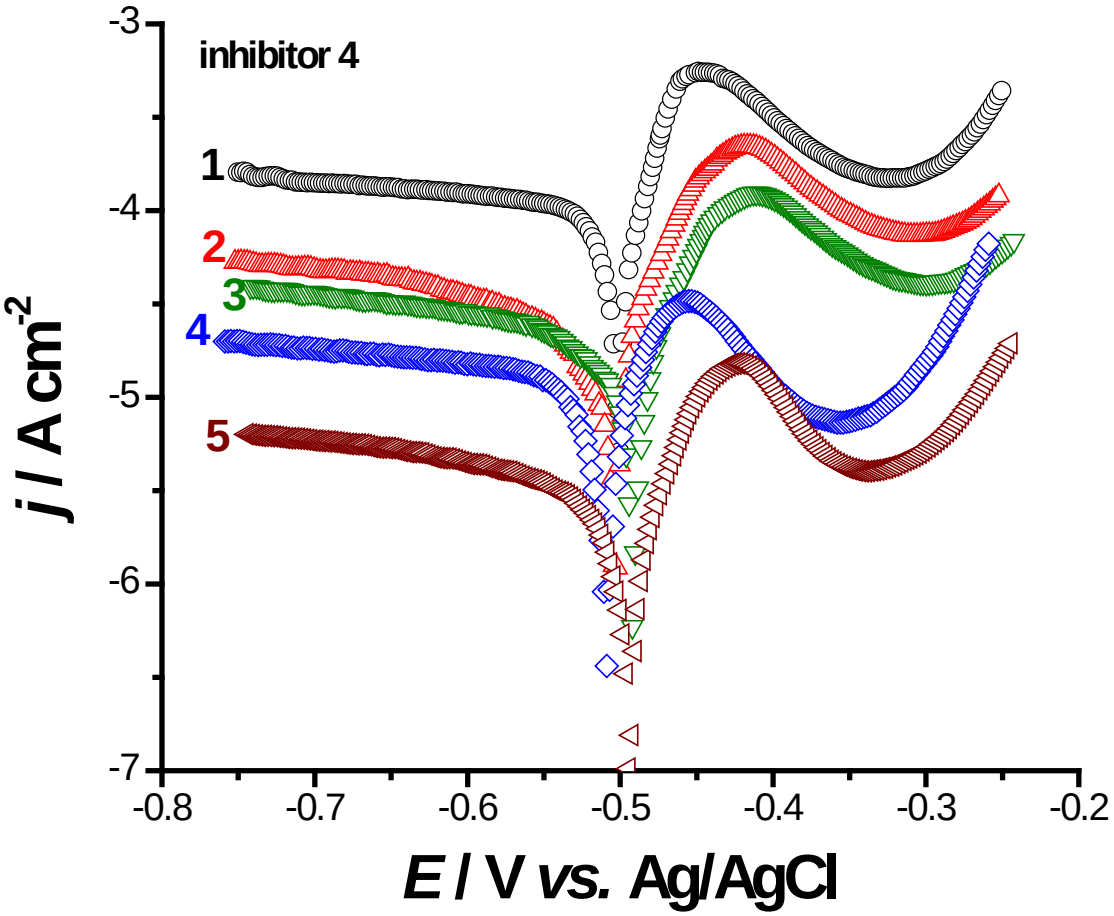

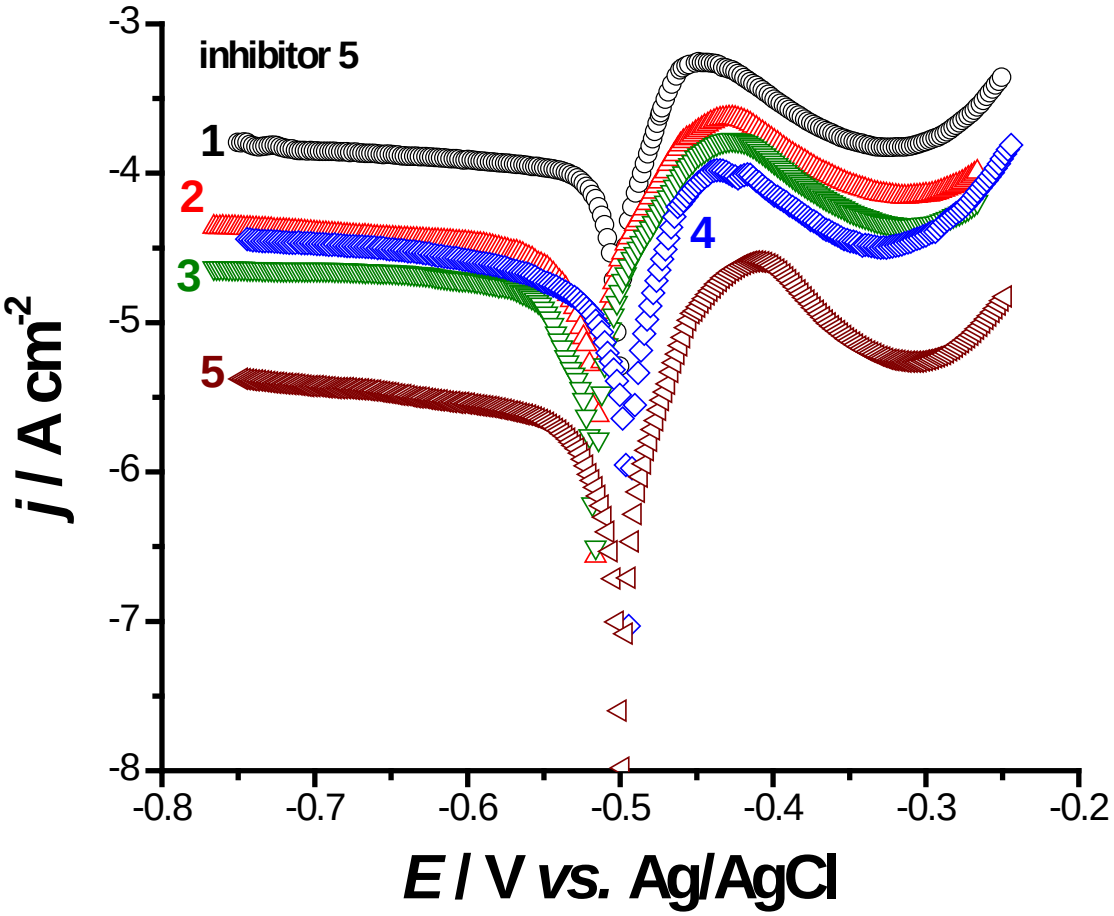

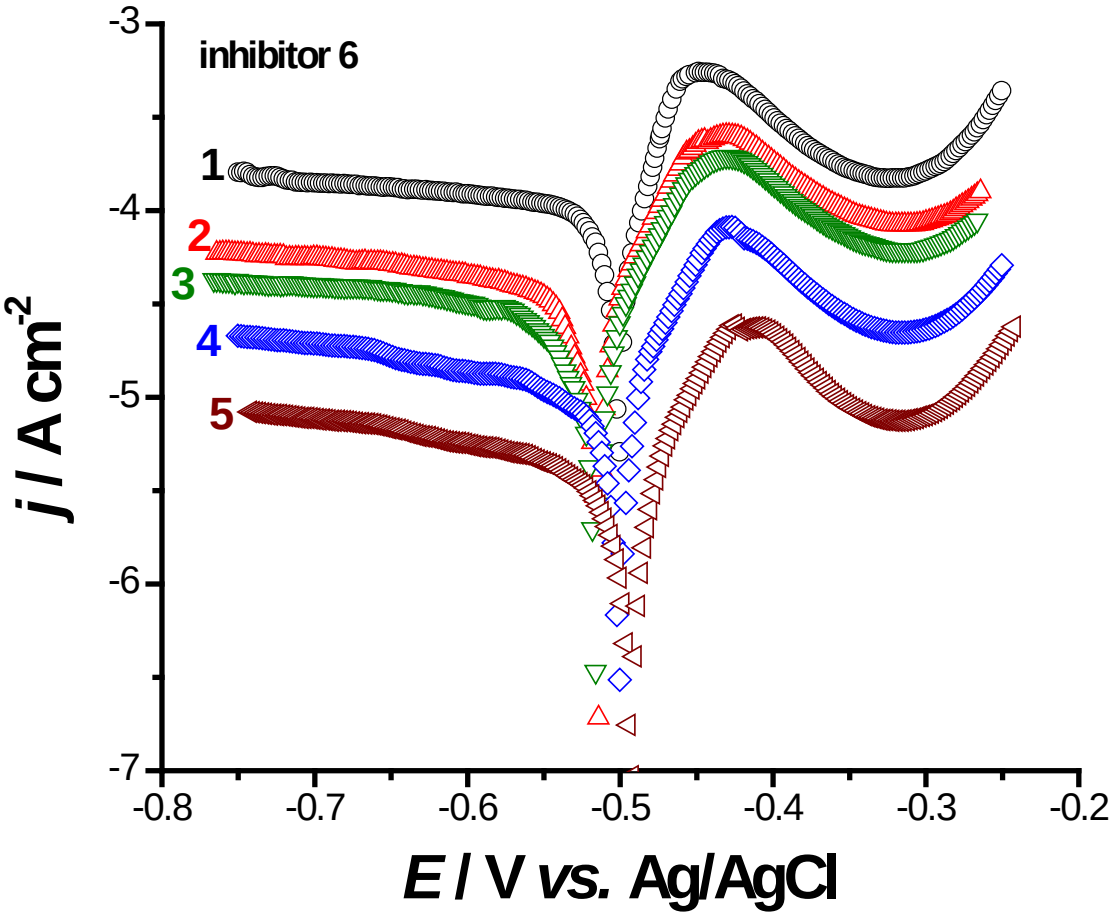

Fig. 5. Cathodic and anodic polarization curves for Cu in 1.0 M NaOH solution devoid of and containing various concentrations (ca. 0.1 – 1.0 mM) of inhibitors **3**, **4**, **5**, or **6**. Measurements were carried out at a scan rate of 5.0 mV s^{-1} at 25 ^{o}C. (1) 0.0 M inhibitor; (2) 0.1 mM inhibitor; (3) 0.2 mM inhibitor; (4) 0.5 mM inhibitor; (5) 1.0 mM inhibitor.

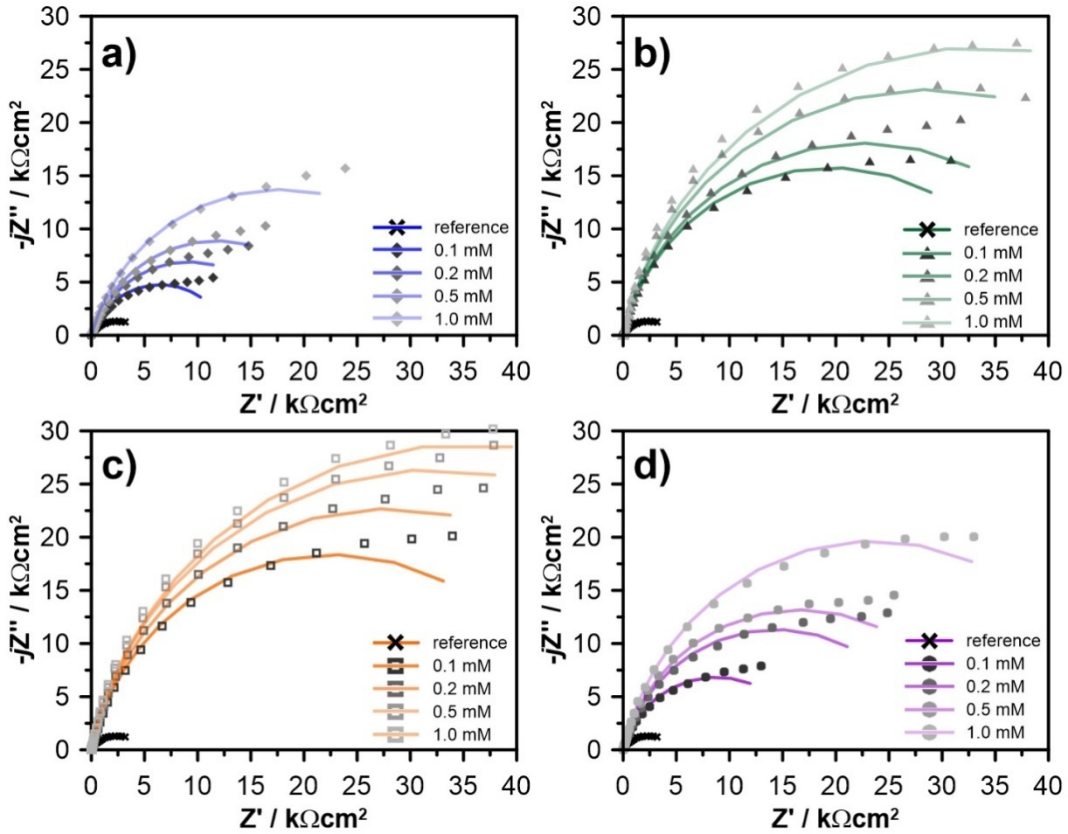

Fig. 6. Nyquist impedance plots for Cu exposed in 1M NaOH solutions with various concentrations (0.1 – 1.0 mM) of investigated inhibitors: a) (3); b) (4); c) (5) and d) (6).

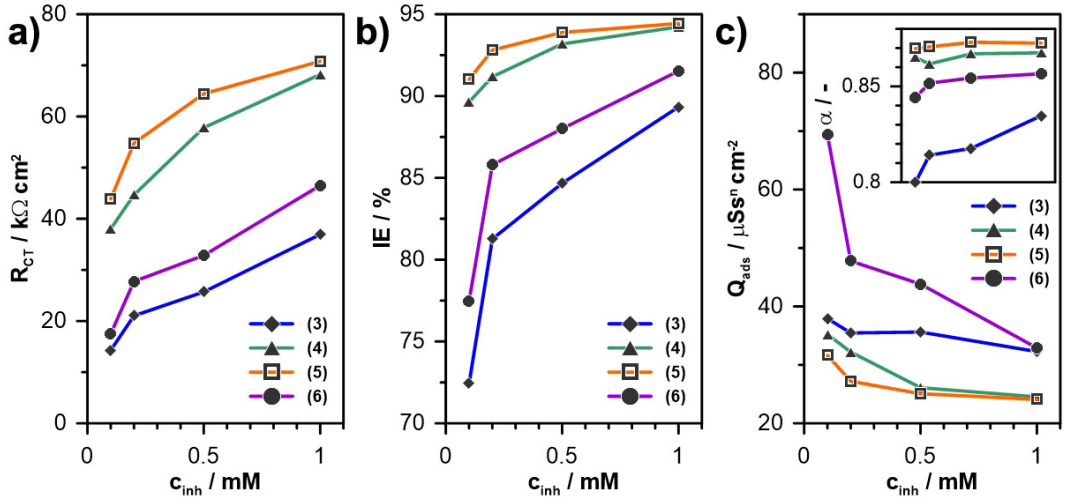

Fig. 7. Comparison of the inhibitory action as a function of corrosion inhibitor concentration based on impedance studies: a) charge transfer resistance R_{CT}; b) inhibition efficiency IE; c) inhibitor film quasi-capacitance, CPE exponent α in the inset.

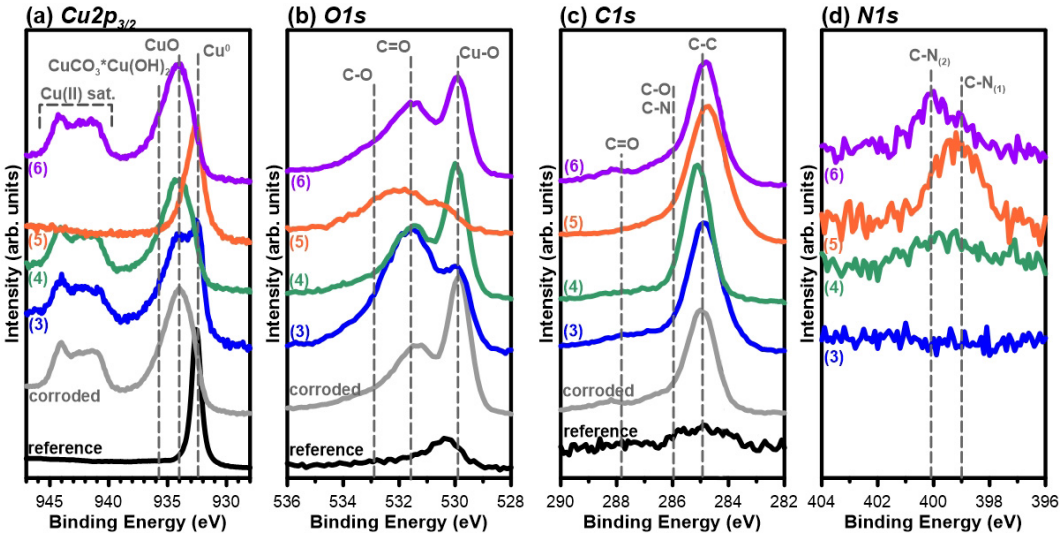

Fig. 8. High-resolution XPS spectra recorded in energy range of: (a) *Cu2p*$_{3/2}$, (b) *O1s*, (c) *C1s* and (d) *N1s* peaks for polished electrode (reference) and electrodes pre-exposed in corrosive media in absence (corroded) and presence of corrosion inhibitor molecules **(3-6)**.

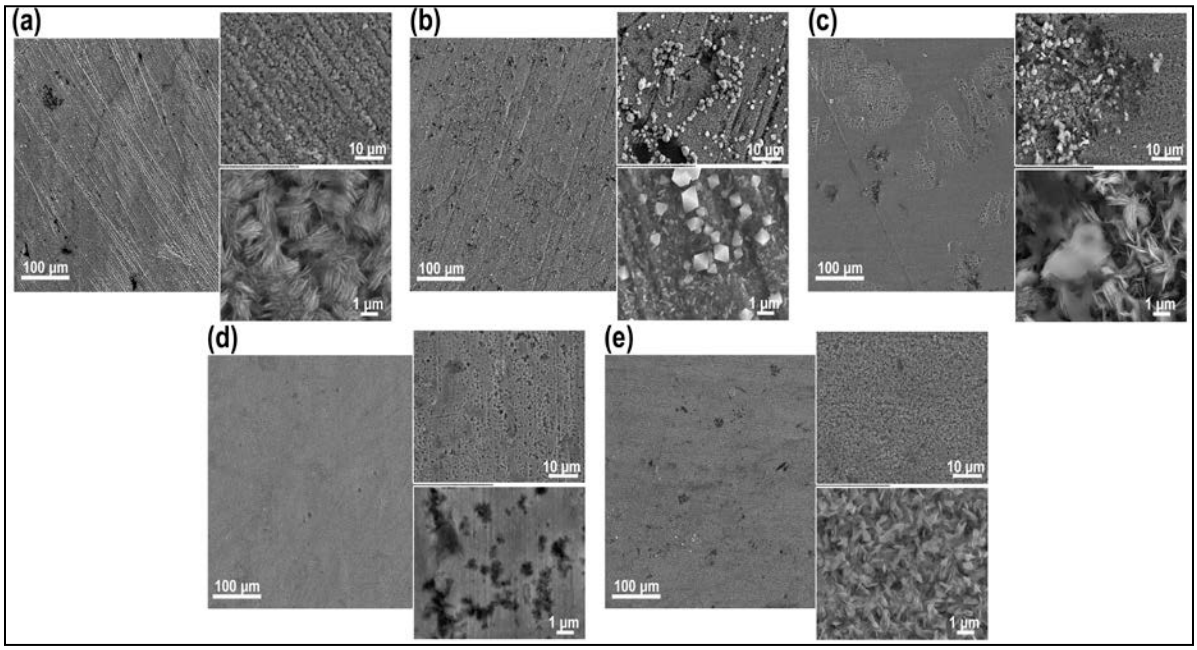

Fig. 9. SEM micrographs performed for pre-exposed Cu samples in alkaline electrolyte: (a) in absence of corrosion inhibitor; (b-e) with addition of corrosion inhibitor **(3)**, **(4)**, **(5)** or **(6)** respectively (Magnification x150, x1500 and x10000).

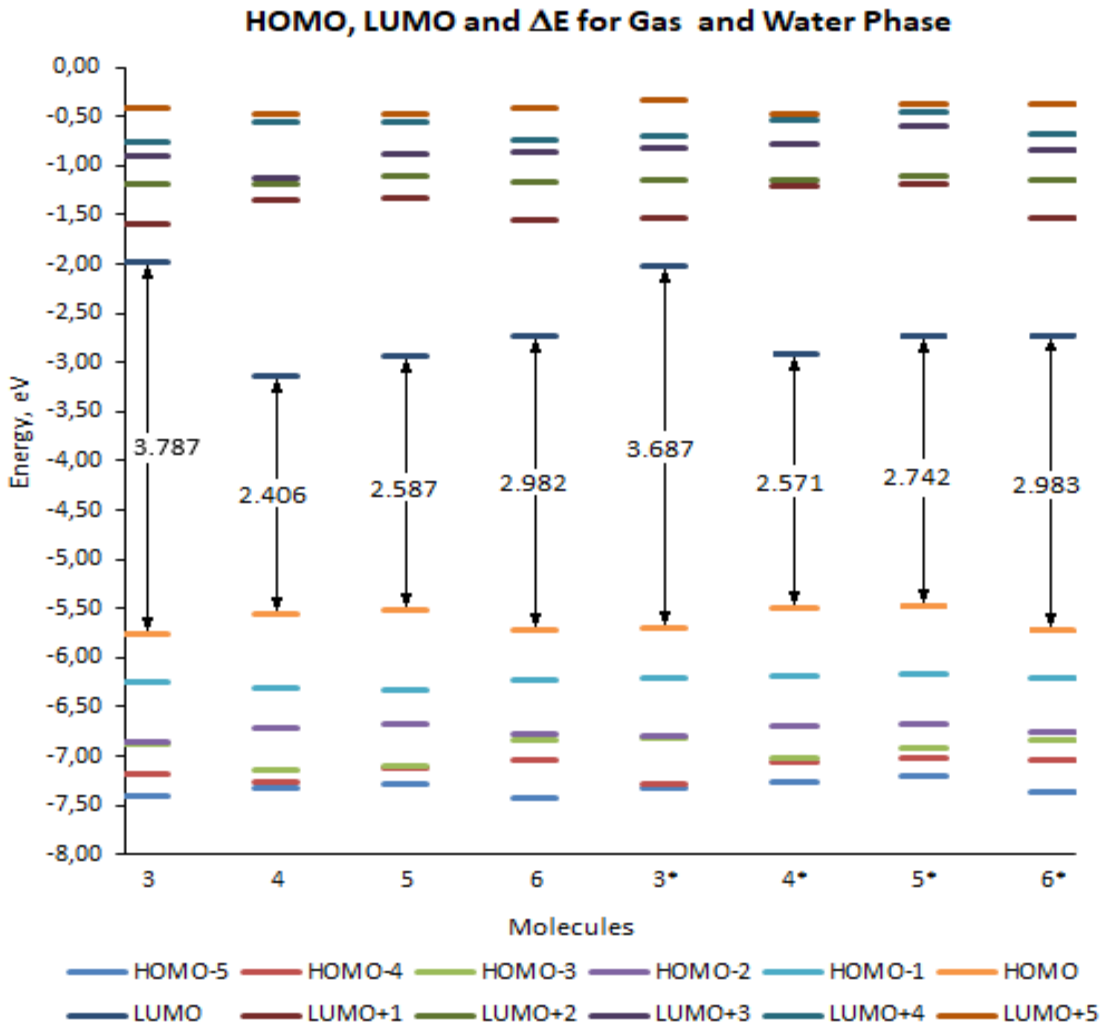

Fig. 10. The calculated E_{HOMO}, E_{LUMO} and energy gap (ΔE) parameters for gas phase and solvent phase (*) of neutral molecules using B3LYP/6-311G(d,p) method.

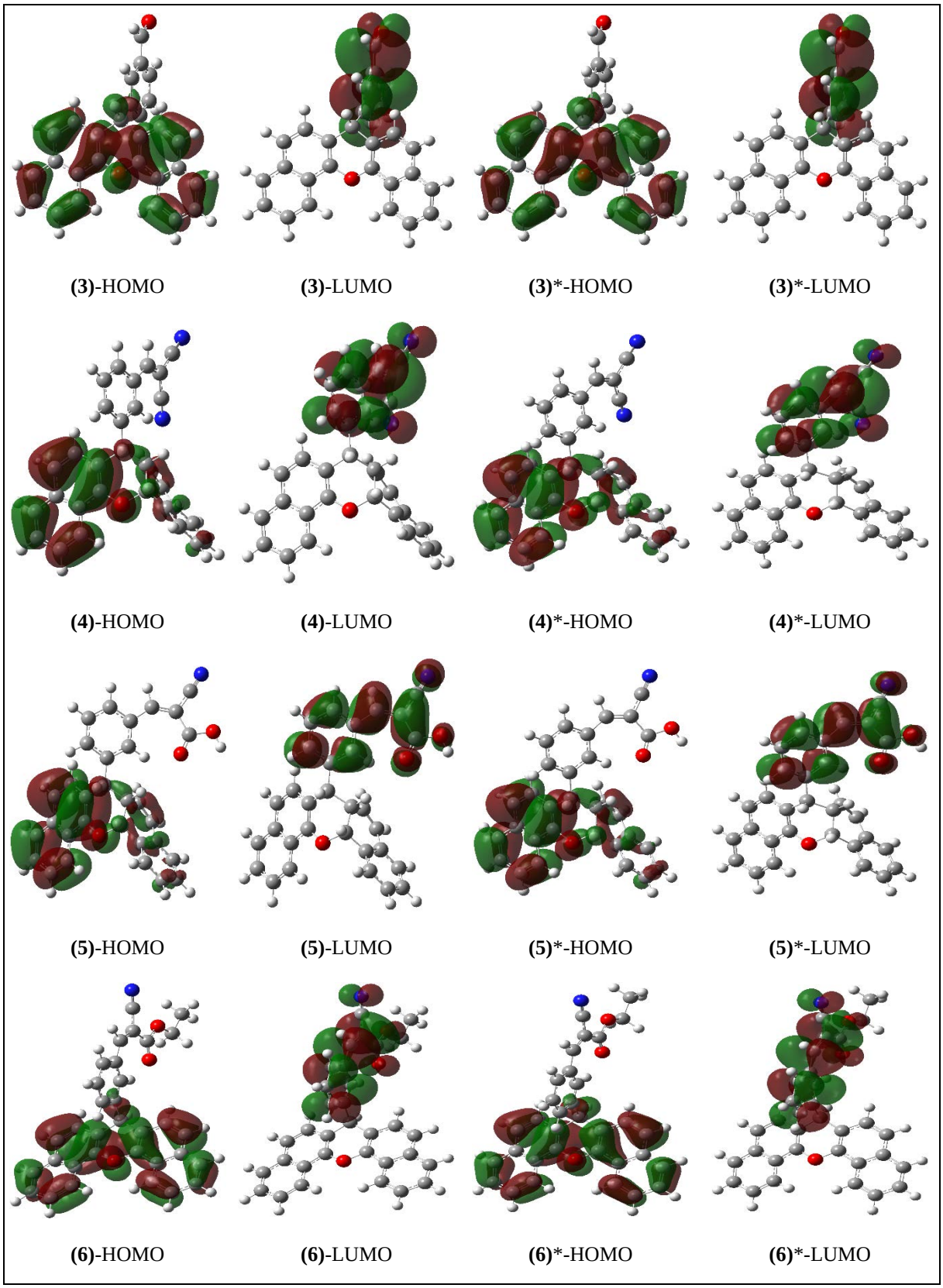

Fig.11 The frontier MOs molecules by using DFT/B3LYP/6-311G(d,p) basic set for notr and water (*) phase.

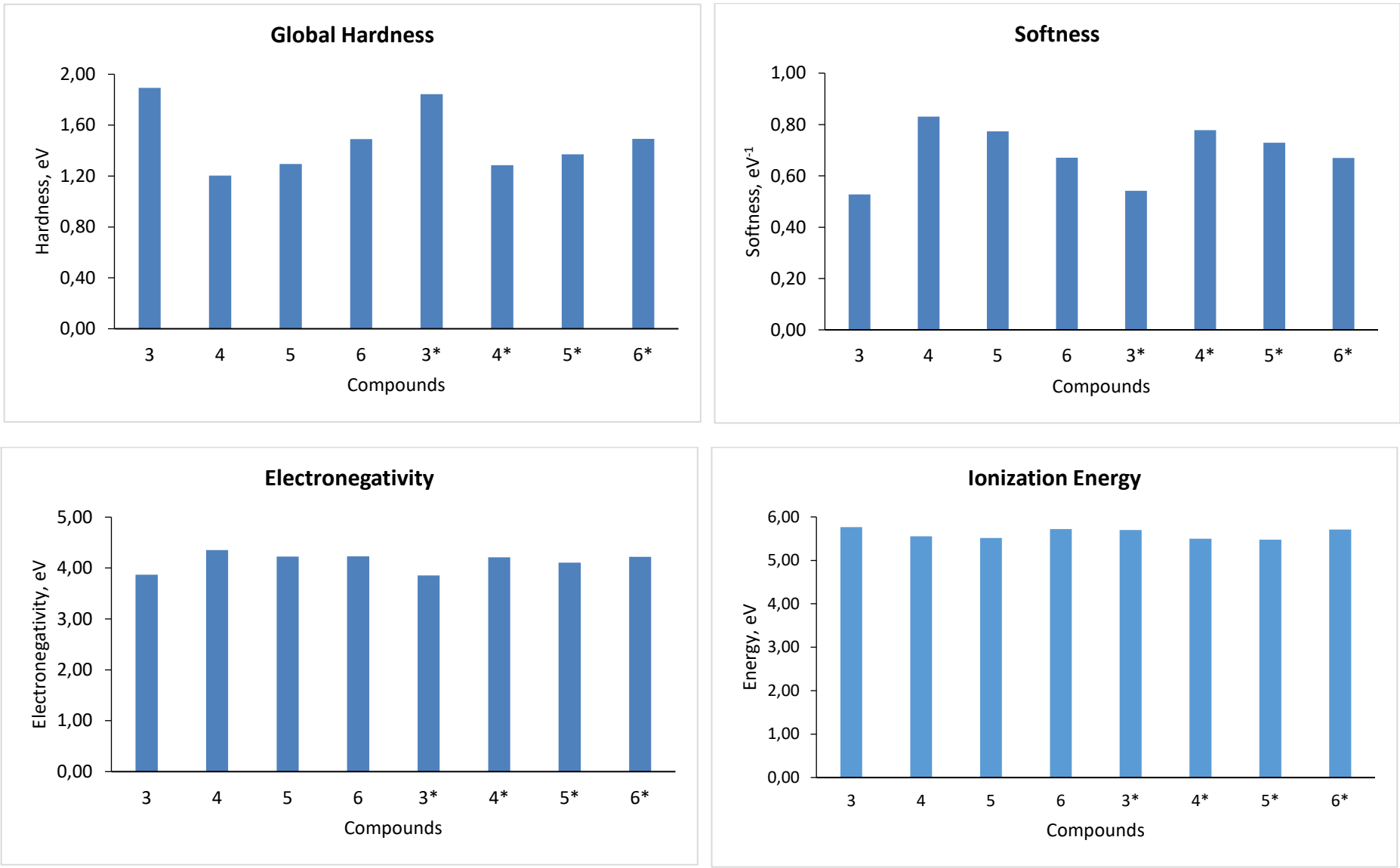

Fig. 12. The calculated quantum chemical parameters ***for gas and water (*) ph***ase using ***B3LYP/6-311G(d,p) method.***

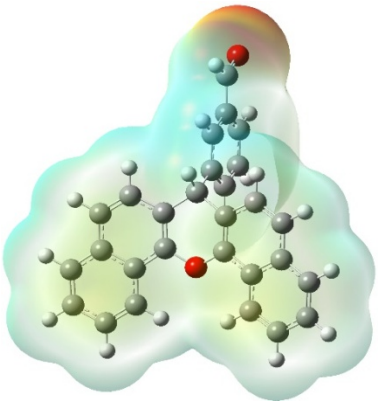	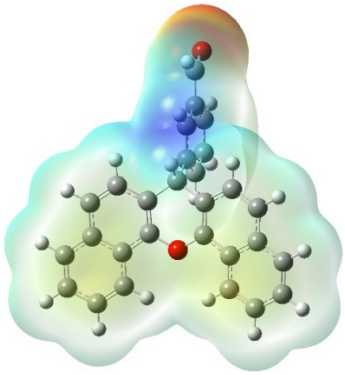
3	**3***
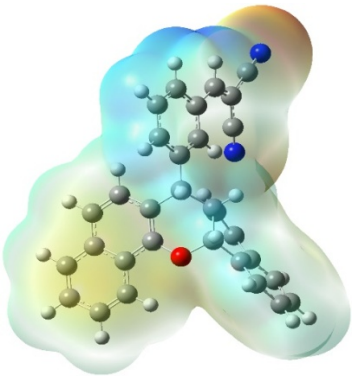	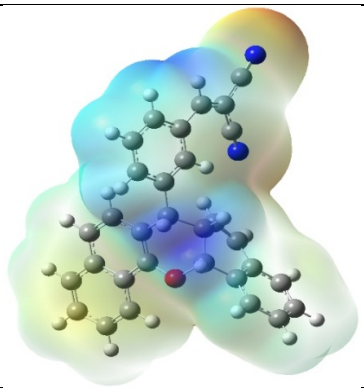
4	**4***
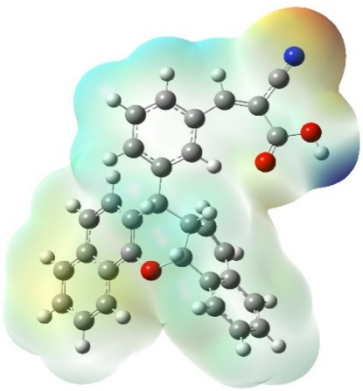	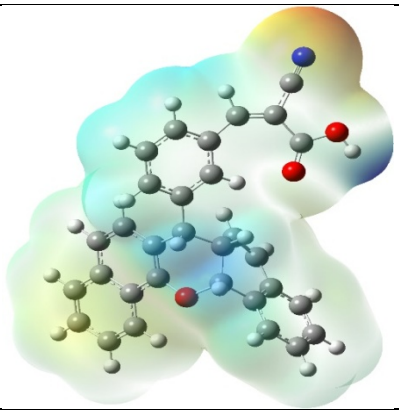
5	**5***

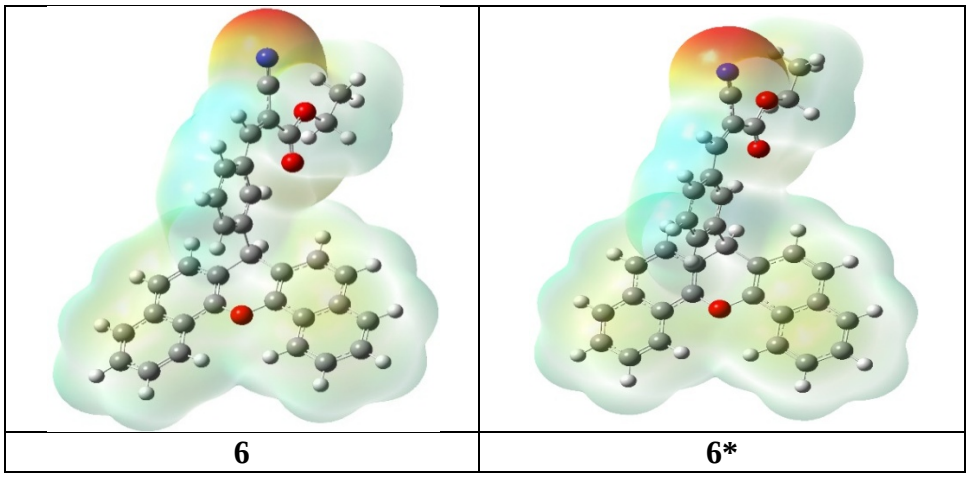

*Solvent phase: Water

Fig. 13. Molecular electrostatic potential (MEP) surface of molecules **(3-6)** by using DFT/B3LYP/6-311G(d,p) basic set for notr and solvent phase.

Table 1

Various electrochemical kinetic parameters derived from polarization measurements (Figure 5) employing Tafel extrapolation method.

Inhibitor	**[Inhibitor] / mM**	E_{corr} **/ mV *vs.* Ag/AgCl**	j_{corr} **/ mA cm^{-2}**	β_a **/ mV dec^{-1}**	ε**%**
3	**0.0**	-500	3.4×10^{-2}	31	---
	0.1	-514	2.1×10^{-2}	59	38.2
	0.2	-516	1.6×10^{-2}	63	52.9
	0.5	-502	8.3×10^{-3}	62	75.6
	1.0	-492	2.8×10^{-3}	67	91.8
4	**0.1**	-503	1.6×10^{-2}	53	52.9
	0.2	-491	1.1×10^{-2}	56	67.6
	0.5	-510	5.0×10^{-3}	47	85.3
	1.0	-495	9.5×10^{-4}	41	97.2
5	**0.1**	-516	1.5×10^{-2}	53	55.9
	0.2	-515	1.07×10^{-2}	58	68.5
	0.5	-494	4.1×10^{-3}	26	87.9
	1.0	-498	4.4×10^{-4}	32	98.7
6	**0.1**	-496	1.7×10^{-2}	31	50.0
	0.2	-476	1.4×10^{-2}	29	58.8
	0.5	-477	6.8×10^{-3}	31	80.0
	1.0	-446	1.9×10^{-3}	30	94.4

Table 2

Surface chemical composition based on *Cu2p3*, *O1s*, *C1s* and *N1s* spectral deconvolution (values in at. %).

		BE (*eV*)	Polished	Corroded	Cu-(3)	Cu-(4)	Cu-(5)	Cu-(6)
Cu2p$_{3/2}$	**Cu^0**	932.8	93.3	1.7	1.9	2.8	2.7	2.0
	CuO	934.0	0.3	10.5	1.4	3.6	0.4	4.4
	$CuCO_3$ *$Cu(OH)_2$	935.6	--	5.2	1.1	4.4	--	3.8
O1s	**Cu-O**	529.9	1.8	17.7	4.8	13.8	0.6	11.7
	C-O	531.7	1.1	17.3	12.1	11.0	3.5	10.9
	C=O	532.9	--	4.3	3.5	4.5	3.4	8.9
C1s	**C-C**	284.8	2.2	31.3	51.5	29.3	63.9	38.1
	C-O/CN	285.9	1.3	6.9	13.4	19.6	12.4	10.3
	C=O	286.7	--	5.1	10.3	9.4	10.1	7.5
N1s	**$C\text{-}N_{(1)}$**	399.2	--	--	--	1.6	3.0	0.4
	$C\text{-}N_{(2)}$	399.9	--	--	--	--	--	2.0

Table 3

Some quantum chemical parameters calculated for the studied inhibitor molecules in the ***gas and solvent phase*** by using ***B3LYP/6-311G(d,p) method.***

Molecule	DM, Debye	ω, eV	TMAC, e	μ, eV	MV, cm^3/mol
3	3.200	3.954	-1.434	-3.870	248.261
4	5.674	7.868	-1.426	-4.351	318.398
5	3.386	6.895	-1.815	-4.224	329.138
6	3.524	6.006	-2.211	-4.232	326.312
3*	3.809	4.032	-1.544	-3.856	310.062
4*	9.269	6.895	-1.597	-4.220	346.464
5*	5.009	6.146	-1.959	-4.105	325.445
6*	4.542	5.969	-2.406	-4.211	355.934

*Solvent phase: Water

Table 4

Calculated Mullikennegative atomic charges on oxygen and nitrogen atoms of molecules by using B3LYP/6-311G(d,p) basic set.

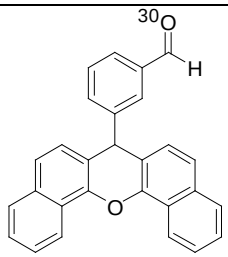

3

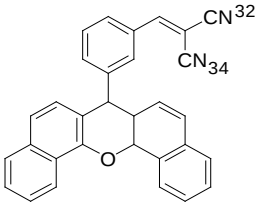

4

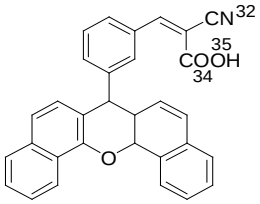

5

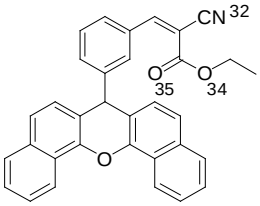

6

Molecule	Atom	Mulliken Charge, e	Molecule	Atom	Mulliken Charge, e
3	O30	-0.286	**3***	O30	-0.344
4	N32	-0.209	**4***	N32	-0.277
	N34	-0.219		N34	-0.263
5	N32	-0.225	**5***	N32	-0.297
	O34	-0.343		O34	-0.364
	O35	-0.314		O35	-0.358
6	N32	-0.231	**6***	N32	-0.312
	O34	-0.333		O34	-0.348
	O35	-0.366		O35	-0.391

*Solvent phase: Water